JAERI-Tech
99-032

A STUDY ON DENSITY, MELTING POINT, THERMAL EXPANSION, CREEP, THERMAL DIFFUSIVITY AND THERMAL CONDUCTIVITY OF THE SIMULATED ROCK-LIKE OXIDE (ROX) FUELS

March 1999

Kazuaki YANAGISAWA, Toshihiko OHMICHI*,
Noriko SHIRASU, Tadasumi MUROMURA
and Tetsushi MATSUDA*

日本原子力研究所
Japan Atomic Energy Research Institute

本レポートは，日本原子力研究所が不定期に公刊している研究報告書です。
入手の問合わせは，日本原子力研究所研究情報部研究情報課（〒319－1195 茨城県那珂郡東海村）あて，お申し越しください。なお，このほかに財団法人原子力弘済会資料センター（〒319－1195 茨城県那珂郡東海村日本原子力研究所内）で複写による実費頒布をおこなっております。

This report is issued irregularly.
Inquiries about availability of the reports should be addressed to Research Information Division, Department of Intellectual Resources, Japan Atomic Energy Research Institute, Tokai-mura, Naka-gun, Ibaraki-ken 〒319－1195, Japan.

編集兼発行　日本原子力研究所

JAERI-Tech 99-032

A Study on Density, Melting Point, Thermal Expansion, Creep, Thermal Diffusivity and Thermal Conductivity of the Simulated Rock-like Oxide (ROX) Fuels

Kazuaki YANAGISAWA, Toshihiko OHMICHI*, Noriko SHIRASU+, Tadasumi MUROMURA++ and Tetsushi MATSUDA**

Department of Nuclear Energy System
Tokai Research Establishment
Japan Atomic Energy Research Institute
Tokai-mura, Naka-gun, Ibaraki-ken

(Received February 22, 1999)

A new type of fuel, that is, rock-like oxide (ROX) fuel composed of PuO_2-SZR (stabilized zirconia)-$MgAl_2O_4$ is under development at JAERI. To prepare the data base, the simulated ROX fuel in which original PuO_2 was replaced by UO_2 was fabricated and brought to out-of-pile tests. Main remarks obtained within this experimental scope are:

(1) It was found from the present study that the simulated ROX fuel was successfully fabricated.

(2) The gas immersion density of the simulated ROX fuels had values ranging from 4.9 to 5.4 g/cc, those were of order of about 47-52% of that of UO_2. Increase of SZR makes the simulated ROX fuel dense to the magnitude of 60% while that of $MgAl_2O_4$ makes the simulated ROX fuel coarse to the magnitude of about 30%.

(3) Melting point of the simulated ROX fuel was revealed to be 1,911±39℃, about 30% lower than that of UO_2 fuel.

(4) The difference in linear thermal expansion (LTE) between the simulated ROX fuel and the UO_2 fuel was little up to temperatures of 1,500℃. The LTE was increased with the increase of SZR.

+ Department of Materials Science
++ Department of Environmental Safety Research
* Research Organization for Information Science & Technology
** Nuclear Fuel Industries, Ltd.

(5) The creep rate of simulated ROX fuel was strongly dependent on the amount of $MgAl_2O_4$, where the increase of $MgAl_2O_4$ of order of 20% in weight caused reduction of the creep rate of order of about 80% at temperatures between 1,300 and 1,400℃. Regarding this, the role of Al_2O_3 dissolved in $MgAl_2O_4$ is important. The creep propensity expressed by stress index, that is, the ratio of deformation rate to *log* (stress) was similar between the simulated ROX fuel and UO_2 fuel.

(6) The magnitude of hardness (Hv) was sensitive to the Al_2O_3 contained in $MgAl_2O_4$, hence the increase of Al_2O_3 made the simulated ROX fuel more hard. Hv in the simulated ROX fuel is significantly greater than that of UO_2 at temperatures <300℃.

(7) The difference in thermal diffusivity between the simulated ROX fuel and the UO_2 was not so significant. Similarly, the difference in thermal diffusivity between the simulated ROX fuel and Gd_2O_3 -doped UO_2 up to 10wt% was also little.

(8) The difference in thermal conductivity between the simulated ROX and UO_2 fuel is little. Degradation of the thermal conductivity occurred by the increase of SZR.

(9) Among three candidates of the simulated ROX fuels studied in the present paper, the sample consisted of 26wt%UO_2-24wt%SZR-50wt%$MgAl_2O_4$ seems to have the most feasible performance for future studies.

Keywords: ROX fuel, Density, Melting Point, Thermal Expansion, Creep, Thermal Diffusivity, Thermal Conductivity

模擬岩石型(ROX)燃料の密度、融点、熱膨張、クリープ、熱拡散及び熱伝導率に関する研究

日本原子力研究所東海研究所エネルギーシステム研究部
柳澤　和章・大道　敏彦*・白数　訓子+・室村　忠純++・松田　哲志**

(1999年2月22日受理)

日本原子力研究所は岩石型(ROX)燃料と称し、PuO_2—安定化ジルコニア(SZR)—$MgAl_2O_4$で構成される新型燃料を開発中である。この燃料に関するデータベースを構築するため、元々のPuO_2をUO_2で代替した模擬岩石型燃料を製造し炉外試験に供した。本実験の範囲内で得られた主たる知見は以下のとおりである。

(1) 研究の結果、模擬岩石燃料は所期の目的のとおり製造されたことが分かった。

(2) 模擬岩石燃料のガス置換密度は、4.9から5.4g/ccの範囲であり、その値はUO_2の47-52%であった。SZRの増加で模擬岩石燃料の燃料密度は60%まで増加した、一方$MgAl_2O_4$(スピネル)の増加で模擬岩石燃料の燃料密度は30%まで減少した。

(3) 模擬岩石燃料の融点は1,911±39℃であり、UO_2燃料の融点より30%低かった。

(4) 模擬岩石燃料とUO_2燃料の線膨張係数（LTE）は、温度1500℃まで差異はなかった。線膨張係数の値はSZRの増加と共に大きくなった。

(5) 模擬岩石燃料のクリープ速度は$MgAl_2O_4$に強く依存した。即ち、温度1,300から1,400℃の間で、$MgAl_2O_4$の量を20%増加させたところ模擬岩石燃料のクリープ速度は約80%低下した。これに関しては、$MgAl_2O_4$の構成成分であるAl_2O_3の働きが重要である。応力指数（変形速度と対数で表示した応力との比）で評価したクリープ特性では、模擬岩石燃料とUO_2の間に類似性が見られた。

(6) 硬度(Hv)は$MgAl_2O_4$に含まれるAl_2O_3に敏感で、その量の増加と共に模擬岩石燃料は硬くなった。温度300℃までの範囲で、模擬岩石燃料とUO_2の硬度を比較したが、前者は後者に較べ著しく大きかった。

東海研究所：〒319-1195 茨城県那珂郡東海村白方白根2-4
+　物質科学研究部
++　環境安全研究部
*　（財）高度情報科学技術研究機構
**　原子燃料工業（株）

(7) 熱拡散率に関して、模擬岩石燃料と UO_2 との間に大きな差異はない。同様に、模擬岩石燃料と Gd_2O_3 を 10wt%まで添加した UO_2 燃料との間の熱拡散率にも差異はなかった。

(8) 模擬岩石燃料の熱伝導度と UO_2 のそれとに差異はなかった。SZR を増加させると模擬岩石燃料の熱伝導度は悪くなる。

(9) 模擬岩石燃料として本実験で使用した３試料のうち、26wt%UO_2-24wt%SZR-50wt%$MgAl_2O_4$ からなる試料がこれからの性能ふるまい研究に最も有望である。

Contents

目　　次

TABLES, FIGURES and PHOTOGRAPHS

TABLES

FIGURES

PHOTOGRAPHS

(i) Sp.#16, 24wt%UO_2-23wt%SZR-$MgAl_2O_4$

Photo. 2 Morphology of three test specimens provided for MP test done by thermal arrest method:
(a) Sp.#1, 100wt%$MgAl_2O_4$,(b) Sp.#2, 32wt%SZR-$MgAl_2O_4$,
(c) Sp.#3, 56wt%SZR-$MgAl_2O_4$,(d) Sp.#5, 100wt%SZR

This is a blank page.

1. Foreword

In conventional light water reactors (LWRs), either a UO_2 fuel or mixed oxide fuel (MOX) made of PuO_2 incorporated into UO_2 is using worldwide. As energy source a further efficient utilization of the plutonium produced at LWR by means of the reprocessing is necessary from the viewpoint of fuel recycling [1].

To date, however, there existed an excess plutonium especially from dismantled nuclear warheads those are stockpiling now of order of 100 tons both in USA and in Russia [2]. To use and reduce the stockpiled plutonium (Pu) from the viewpoint of NPT (the Non-Proliferation of Nuclear Weapons), there are several options. One of promising way is to burn Pu in form of the rock-like oxide (ROX) fuels in LWR (that is, one-time Pu consumption).

The Japan Atomic Energy Research Institute (JAERI) has been studying the ROX fuels since year of 1994 by its own fabrication technique [3]. The one of advantage in the use of ROX fuel is that a spent ROX fuel can be disposed directly with safe after the burn in LWR because the fuel is composed of very stable matrix against a fission product (FP) migration. So, the disposition of spent ROX fuel is quite economic and safe [4].

The ROX fuel under development in JAERI consisted of several mineral components represented either by (1) PuO_2-ZrO_2 (Y)-Al_2O_3-$MgAl_2O_4$ or by (2) PuO_2-ThO_2-Al_2O_3-$MgAl_2O_4$. Where, ZrO_2 (Y) is so called a stabilized zirconia consisted of ZrO_2, Y_2O_3 and Gd_2O_3 as main components. The addition of rare earth materials such as Y_2O_3 is to avoid ZrO_2 from cracking and fracture at elevated temperature of around 1,000℃. Hereinafter it will be abbreviated as SZR. Differing from the conventional UO_2 or MOX fuels, the ROX fuel is made of multi-component structures. This makes a complicated situation for understanding physical characteristics from thermal and mechanical points of view. Data base necessary to build up the modeling of in-core fuel behavior is significantly poor, to date.

Due to aforementioned backgrounds, the out-of-pile experiments to increase physical fundamental data on the ROX fuel were planned to carry out. The data will be utilized in future to modify the computer code FPRETAIN [5] for the ROX fuel, which was originally designed to predict the UO_2 fuel behavior not only under the steady-state operation but also under the reactivity initiated accident

(RIA). The present paper is to describe the results of out-of-pile experiments.

2. Experimental Methods and Results

2.1 Fabrication of the Test Specimens

In the present study, due not only to a limitation of fabricating capability but also to a difficulty from handling management at the laboratory, a plutonium dioxide (PuO_2) as a fissile material was replaced by a uranium dioxide (UO_2). It is believed, however, that physical characteristics between UO_2 and PuO_2 are very similar so that results to be obtained from this study should useful for characterization of the ROX fuel. In the followings, the authors denoted the test specimen as the simulated ROX fuel.

At the present study, 9 different kinds of test specimens as listed in **Table 1** were used. Nominally, at JAERI, four different kinds of oxide powders (SZR, Al_2O_3, MgO, UO_2) were dissolved in the nitric acid solution and blended into 9 different lots after drying. At the Nuclear Fuel Industries Co. Ltd., Japan, the powders were pressed into the green pellets in an atmospheric environment. After pressing, 9 kinds of green pellets were sintered all at 1750℃ for 4 hours (1750℃/4h) under the reduced environment made of hydrogen mixed with nitrogen gas (N_2+3H_2). As seen from the previous table, sintered specimens had the outer diameter (D) of 7.8 ~9.9mm, the length (L) of 8.0~10.3mm and the L/D of 0.8~1.2, respectively. The dimension is roughly similar to that of the conventional UO_2 fuel pellet provided to the commercial pressurized water reactors (PWRs). An error band shown in the table was obtained from the statistics.

(1) SZR

The main role of SZR is to confine fissile (UO_2) and becomes as the core part of the simulated ROX fuel. In the followings, an existing ratio of individual compound will be shown by two ways such as 1) molecular percentage (abbreviated as mole %) and 2) weight percentage (abbreviated here as wt%). The compound SZR is originally stabilized zirconium dioxide (ZrO_2) designed by 88.8% ZrO_2-11%Y_2O_3-0.2%Gd_2O_3 (mole%) and denoted hereinafter as SZR or sometimes simply as Zr. From metallurgical point of view, SZR has the same structure as UO_2 (fluorite) so that the two were dissolved easily at sintering stage.

(2) $MgAl_2O_4$

The main role of $MgAl_2O_4$ (spinel) as the inert matrix is aimed at increasing a thermal conductivity of the simulated ROX fuels. In order to fabricate the spinel, two kinds of powders of Al_2O_3 and MgO were prepared and dissolved in the nitric acid solution and then dried for mechanical blending. At a design stage one expected the formation of Al_2O_3 (corundum) and $MgAl_2O_4$ (spinel) compounds through the mixing of two powders but the resultant compound after sintering was revealed to be $MgAl_2O_4$ only.

By a scanning electron microscopy (SEM), the microstructures of 9 kinds of ROX fuel pellets were studied. They are shown in **Photo. 1**. Specimen #1 (hereinafter abbreviated simply as "sp.#1".) and sp.#5 in the photograph respectively show a single phase of $MgAl_2O_4$ and that of SZR. The remainders showed microstructures of dispersion type fuels derived from typical eutectic reactions. One can understand that sp.#2 consisted of the bright and the dark areas composed of the SZR phase and the $MgAl_2O_4$ one. As clear from the sp.#12, #13 and #16, an addition of UO_2 caused the increase of bright (SZR) area, where the dissolution of UO_2 into the SZR occurred. In other words, the UO_2 was confined successfully into the SZR compound and became the core of the simulated ROX fuels. SZR has an important role to confine the fissile materials as well as to confine all fission products during irradiation. Additionally, one expected SZR as the strong and safe barriers against the environment during the disposition of the ROX fuels.

In the subsequent discussions, the three kinds of simulated ROX fuels containing UO_2 compound (sp.#12, sp.#13, sp.#16) were denoted sometimes as "fuel core". In the contrast, the three kinds of test specimens containing no UO_2 (sp.#02, #03, #6) were denoted sometimes as "inert matrices". Sometimes, a direct comparison of performance between the two groups is made. The property of simulated ROX fuel is also compared with that of UO_2 fuel.

2. 2 X-ray Diffraction Analysis

The purpose of X-ray diffraction (XRD) analysis was to identify crystalline structures of the test specimens by means of the pattern recognition method. Resultant data are shown in **Fig. 1**. It is notable that the sp. #1 shown in the top of figure was originally blended by 72wt%Al_2O_3 and 28wt%MgO powders and found to be a single phase of $MgAl_2O_4$ after sintering. While, the sp. #5 was made of 100wt% SZR. XRD of the former showed 7 clear peaks between diffraction angle

40 and 80 degrees and that of the latter showed 4 clear peaks between the same angles. Taking into consideration of those peaks as the basis of pattern recognition, XRD analysis was made.

It was revealed that the remainders (sp.#2, sp.#3, sp.#4 and sp.#6) consisted of the fundamental patterns. Their grain sizes were measured separately and found to be <10 μm. In the bottom of figure, XRD of the simulated ROX fuel (UO_2-SZR-$MgAl_2O_4$) is shown. Around 60 degrees, clear peaks relating to the SZR-UO_2 solid solution were observed.

With respect to the sp.#6 (20mol%SZR-$MgAl_2O_4$) and the sp.#16 (10mol%UO_2-18mol%SZR-$MgAl_2O_4$), no Al_2O_3 component was detected, even though the fact of excess amounts of Al_2O_3 (mol%) between them. Namely, the excess of ratio in stoichiometry (Al_2O_3: MgO=1:1) occurred at the beginning of sintering. Lastly, the final compound formed by any mixture of Al_2O_3 and MgO was $MgAl_2O_4$ alone. According to the phase diagram [6] a complete dissolution of Al_2O_3 into $MgAl_2O_4$ was possible to occur.

The sp.#6 (Al_2O_3>MgO) was provided for the comparison with the sp. #2 (20mol%SZR-40mol%Al_2O_3-40mol%MgO, hence Al_2O_3=MgO). By using a lattice constant obtained from XRD analysis, we found that the lattice constant of the former was small to the magnitude of 0.7% than that of the latter, implying that the Al_2O_3 was dissolved into $MgAl_2O_4$ perfectly.

In the bottom of figure, XRD of the simulated ROX fuels (#12,#13 and #16) is shown. Basing on SZR peaks of the sp.#5, obtained peaks of them were shifted towards low-angles because of the formation of UO_2-SZR solid solutions (abbreviated as (UO_2-SZR)ss), hence the lattice constants of these were increased. As the magnitude of low-angle displacement was increased with the increase of the value given by $UO_2/(UO_2+SZR)$[16], the lattice constants of the former two were larger than that of the latter.

The crystalline structures of the specimens decided by XRD were summed up in the right-hand column of **Table 2.** The sp.#12 , for example, is composed of the fluorite structure (abbreviated as F) of UO_2-SZR and spinel structure (S). It is clear that the core of the simulated ROX fuel is made of UO_2 dissolved into SZR. It was surrounded by the inert matrix consisted of $MgAl_2O_4$.

2. 3 Fuel Pellet Density

2. 3. 1 Pores and pellet density

During sintering, the pores are born inside the fuel pellets. It is known that the pores affect much on fuel performance under the neutron fluxes at irradiation field. For example, the decrease or increase of the pores during irradiation will cause the densification or swelling inside fuel pellet. Thus, the in-core integrity of ROX fuel was partly dependent on the initial pores existed. It is worthy of mentioning that amounts of pores are strongly influenced by the as-fabricated pellet density.

Regarding a UO_2 fuel used in LWR, the as-fabricated density was 10.41 g/cc (or Mg/m^3), where the theoretical density (TD) was common to known as 10.96 g/cc. Hence, a value given by relation {1-(10.41/10.96)} x 100(%) indicates how much pores (voids) are contained. It is important because as mentioned above they influenced much on fuel integrity when used in the core [7]. To date, a calculated value given by (10.41/10.96) x 100(%) is defined as the percent theoretical density (%TD).

There existed two kinds of the pores; open and close ones. The former connects from inside pellet to outside (surface) directly so that principally it is measurable. As to the case of latter, pores are isolated at inside of fuel matrix then hard to measure. If one can obtain theoretical density of ρ_{th} (g/cc), the pellet bulk density of ρ_m(g/cc) and amounts of open pores (which is denoted here as an open porosity(%)), then amounts of closed pores (that is, the closed porosity(%)) should be evaluated by the relation; closed porosity(%)={1- ρ_m/ ρ_{th} }x100-open porosity(%). As a general tendency it is known that closed pores will increase with the decrease of pellet bulk density. For the case of UO_2 pellet, closed porosity will increase gradually from the density range <95%TD [8].

2. 3. 2 Density of simulated ROX fuels

As similar as a UO_2 fuel, the simulated ROX fuel was sintered. As shown in Photo. 1, not only the fuel core but also the inert matrices contained some amounts of open and closed pores formed during sintering. At moment, we have no effective tools for determining %TD of individual specimens used here. The determination of it is another matter of topics to be done in the future.

Tentatively, what we did here is to obtain the pellet geometrical density (GD). However, it gave a poor information about the pores. To the next, helium gas immersion density (GID) was measured to know rough amounts of the pores.

(1) Pellet geometrical density

GD was measured by the as-fabricated dimension and was listed up in **Table 2** together with statistical error band. A relative small error band means that original pellets were fabricated and dimensioned accurately. GD as a function of the test specimen is shown in **Fig. 2**. The followings were revealed:

- For the inert matrices (from the sp.#1 to the sp.#6), GD ranged from 3.2 to 5.2 g/cc. The increase of GD occurred by the increase of SZR, except #6. Hence the addition of SZR may make the simulated ROX fuel dense. The low density observed in the sp.#6 is attributed to its significant large amounts of pores.
- GD of the simulated ROX fuels were of order of 4.7-5.1g/cc. The value was about half of UO_2. A comparison between the sp.#2 (no UO_2) and the sp.#12 (UO_2) revealed that GD increased from 4.0 to 4.7g/cc. It was repeatedly observed in the sp.#3 and the sp.#13. This implies that GD of the specimen with UO_2 (that is, the simulated ROX fuel) is greater than that of the specimen without UO_2 (that is, the inert matrices). It is possible to occur because the density of UO_2 is a relatively high.

(2) He gas immersion density

After GD measurement, the pellets were fragmented into pieces and brought into a pressurized chamber, where the sorbed gases (N_2 and H_2) were replaced by the pressurized pure helium (He) gas with known volume. Then, a rough volume of initial pores was obtained. This method, however, not enough to know a total volume of pores. There still existed the uncrushed small-sized pores. In Table 2, the GID of 9 specimens is listed. It varied from 3.5 to 5.9 g/cc. Regarding the sp.#1, TD referred from the open literature [9] was 3.55 g/cc instead of the GID of 3.52 g/cc, meaning that uncountable pores are there. The difference between GID and TD revealed was not so significant, therefore, we decided to put GID as TD. This assumption enable us to estimate the rough percentage of remained pores by the relation; {1-(GD/GID)} x 100(%).

Obtained GD and GID are plotted together in **Fig. 3**. The followings were revealed:

- GID of the simulated ROX fuel was roughly 4.9 g/cc for the sp.#12 and 5.4g/cc

for the sp.#13. They are equal to about 47-52% of the density of UO_2 . On the other hand, GID of the inert matrices varied from 3.5 g/cc to 5.2 g/cc. A comparison between the simulated ROX fuel (sp.#12) and the inert matrix (sp.#02) showed that GID of the former was greater to the magnitude of 30± 9%.

- The sp.#6 showed the significant increase of density, hence changed from 2.89g/cc by GD to 4.02 g/cc by GID. It implies that a large number of pores are existed. In fact, estimated pores were 28.1%. It is worthy of mentioning that in this case the original Al_2O_3 and MgO elements did not show the stoichiometric condition because the ratio of Al_2O_3 to MgO was 50:30 in weight. This did not occur in the sp.#16 though it was fabricated similarly. Namely, the sp.#16 had a relative large density of 4.8g/cc and less amounts of pores (1.8%). This inconsistency occurred in the fabrication stage and at present the authors do not understand the cause of mechanism. The importance is that GD sometimes not tell a true density.
- GID is, of course, greater than that of GD. Averaged density of all tested samples was 4.7±0.8 g/cc for GID and 4.4±0.8 g/cc for GD. For the inert matrices, GID varied from 3.5 to 5.9 g/cc according to the increased amounts of SZR. Since, SZR had a function to make ROX fuel dense to the magnitude of 60% in maximum case.

(3) Volumetric ratio between $MgAl_2O_4$ and UO_2 combined with SZR

As revealed by XRD tests, the sp.#1 (3.52g/cc) consisted of a single phase of $MgAl_2O_4$, while the sp.#5 (5.89g/cc) consisted of a single phase of SZR. The remainders were mixtures of the two plus UO_2. To estimate an existence ratio of each components (%) in the remainders, we here neglected the existing pores here and used the lever rule given by the relation: $(M \times m/d)_f \div \{(M \times m/d)_f + (M \times m/d)_s\}$. Where, M is the molecular weight, m the mole number and d the GID. Additionally, suffix "f" means terms related to fluorite components (UO_2, SZR) and "s" means terms related to spinel component ($MgAl_2O_4$), respectively. Results are summed up in **Table 3.** It is revealed that regarding the simulated ROX fuel the volumetric ratio between the inert matrix and the fuel core was 70:30 for the sp.#12 and 51:49 for the sp.#13.

The use of $MgAl_2O_4$ was aimed at increasing the thermal conductivity because of a poor thermal conductivity of SZR and UO_2. Unnecessary increase, however, tended to cause the decrease of fuel bulk density, for example, to a magnitude of

about 30% in the worst case. A low dense fuel in general has a potential to enhance fuel densification at the early stage of irradiation and swelling.

2.4 Melting Point

Generally, the MP of nuclear fuels under reactor operating is one of important design factors, especially from the licensing point of view. In conventional LWR, the MP of UO_2 fuels both under the steady-state operation and under the transient operation is restricted strictly at any burn-up stages. It is also known that the MP has a tendency to decrease with the increasing burn-up due mainly to a formation of fission products (FP), restructuring of the fuel component and so on.

In the present study, MP of the test specimens was measured by the thermal arrest method [10,11]. An apparatus used for this is shown in **Fig. 4**. Firstly, a weighed specimen (about 0.1 g) was mounted on a tungsten heater placed on a vacuum chamber, which had a rectangular shape possessing width by 5mm and length by 100mm. Heat up rate from the room temperature to the MP was about 14℃/s. The two-colored pyrometer was set beneath the tungsten heater to record a change of temperature. The monitored temperature was from the heater but not directly from the test specimen, however, the difference between the two is insignificant. Heat up was made in the adiabatic manner under the inert gas (85%Ar+15%H_2) environment. A sign of melt was expected to confirm by the temperature plateau occurred by a phase transformation mechanism.

Prior to the test, a temperature calibration by using MP-known materials such as Al_2O_3, Y_2O_3 and HfO_2 was carried out. MPs from the tests were 2,067, 2,415 and 2,781℃, while those from literature[12] were respectively 2,054, 2,439 and 2,803 ℃. By using obtained two data sets, the one-by-one calibration line was prepared and the temperatures from the tests were converted into literature data.

Measurements were carried out through the sp.#1 to the sp.#16 except the sp.#4. Representative temperature histories are shown in **Fig. 5**. Differing from our expectation, in most cases, the temperature plateau as a sign of fuel melt could not be recorded clearly, where a sudden drop of temperature at short time span occurred. Therefore, the temperature at just end of the sudden drop readable from the curve was defined as the MP, which might be corresponded to the inception of fuel melt. Overviews of those specimens after the test are representatively shown

in Photo. 2. A rhombic shape of the specimen is the indicative of occurrence of the fuel melt.

The MP is summarized in Table 4. A maximum error band was within ±15℃. The MP of selected 8 specimens was plotted in Fig. 6. The specimen #5 composed of 100wt% SZR gave highest MP of 2,724℃, while the sp.#6 (30wt%SZR-$MgAl_2O_4$) and the sp.#16 (24wt%UO_2-23wt%SZR-$MgAl_2O_4$) showed the lowest MP of about 1,864℃.

(1) Representative melting point of the test specimens

Prior to find out the representative MP not only for the simulated ROX fuels but also for the inert matrices, the sp.#1 and the sp.#5 were omitted because they were inadequate to consider either as the simulated ROX fuels or as the typical inert matrices. Then the followings were obtained.

Specimen	MP (℃)
(1) Inert matrices (sp.#2,#3 and #6)	
SZR-$MgAl_2O_4$	1,908±38
(2) Simulated ROX fuels (sp.#12, #13 and #16)	
UO_2- SZR-$MgAl_2O_4$	1,911±39

The use of UO_2 (MP=2,800-2850℃) did not cause the increase of MP of the simulated ROX fuels. Clearly, there is no big difference between the above two data sources. As MP of the simulated ROX fuel, the temperature of 1,911±39℃ is chosen. Perhaps, the value might not be different much from the ROX fuel consisted of PuO_2-SZR-$MgAl_2O_4$ because the MP of UO_2 fuel is resembled to that of PuO_2.

(2) Comparison with published data

(2-1) Inert matrices

- The MP of the spinel from ref.(6) is 2,105℃ (the eutectic point) as shown in Fig. 7, while that obtained from the present study was 2,102℃. The MP obtained from the present study is the same as that obtained from ref. (6).
- The MP of the SZR (88.8mol%ZrO_2-11mol%Y_2O_3-0.2mol%Gd_2O_3) was decided by ignoring the amounts of Gd_2O_3. The MP of the simplified SZR from ref.(6) is 2,750℃ as shown in Fig. 8, while that obtained from the present study

was 2,724℃. The difference between the two is insignificant.

- The MP of $MgAl_2O_4$-SZR is not known to date. The estimated MP from MgO-ZrO_2 phase diagram (Fig. 9) was nearly 2,100℃. While, the MP from present study ranged between 1,864-1,931℃. The MP obtained from the present study is lower to the magnitude of 169-236℃ than that of the ref. (6).

(2-2) Simulated ROX fuels

- Instead of the UO_2- $MgAl_2O_4$ phase diagram, the phase diagram of UO_2-MgO shown in Fig. 10 and that of UO_2-Al_2O_3 shown in Fig. 11 were referred to. The MP of the former was almost constant having the value of 2,027℃, while the MP of the latter was also almost constant having the value ranged between 1,900 and 1,930℃. This implies that the MP of UO_2-$MgAl_2O_4$ may be existed between 1,827 and 2,027℃ even though occurrence of a slight change of components.
- Instead of the UO_2-SZR phase diagram, the phase diagram of UO_2- ZrO_2 shown in Fig. 12 was utilized. The two elements formed the solid solution around the constant temperature range of 2,600℃.
- The phase diagram of the UO_2-$MgAl_2O_4$-SZR is too complicated to understand. As seen from Fig. 9, the UO_2- ZrO_2 may decrease its MP to form the eutectic solid solution with $MgAl_2O_4$. The final value may be governed strongly by the eutectic point of the UO_2-$MgAl_2O_4$, hence around 1,827-2,027℃. The MP of UO_2-$MgAl_2O_4$-SZR was roughly estimated to be 1,866-1,933℃. The estimated MP coincided with that obtained from the present study.
- As summed up in Fig. 13, MPs obtained from the present study and those obtained from ref. (6) were shown. Two data were resembled. This might be attributed to the eutectic reactions occurred during sintering stage of the inert matrices and the simulated ROX fuels. It is important to say that the increase of MP of the simulated ROX fuels may be impossible to achieve within this experimental scope.

(3) Comparison with UO_2 data

It is worthy of mentioning that the MP of UO_2 in LWR ranged roughly from 2,800 to 2,850℃ at the beginning of life (BOL)[11]. As shown in Fig. 6, the representative MP of simulated ROX fuel of 1,911±39℃ is about 30% lower than that of UO_2. The relative low MP in the former is addressed to the nature of dispersed type multi-component structures designed by the requests from the viewpoint of reactor physics, safety for disposition and many other reasons [3,4,13].

2.5 Thermal Expansion

2.5.1 Measurement

From a viewpoint of fuel mechanical behavior during a reactor operating, a linear thermal expansion (abbreviated here as LTE) of the ROX fuel will be an important factor, especially on the inception of pellet-cladding mechanical interaction (PCMI). For study on LTE of the simulated ROX fuel, an apparatus as shown in **Fig. 14** was prepared. A test specimen was in form of flat pellet, having an outer diameter(D) of 9.08±0.58mm, length(L) of 9.61±0.79mm and L/D of 1.06±0.13, respectively. A sapphire was used for the purpose of data calibration, where LTE of the sapphire was known to be almost linear (about 0.6% at 1,000℃). The sapphire and the test specimen were put together into the furnace settled in the apparatus, then a top of each by a few grams weight suppression was kept. With increasing temperature in furnace under the reduced environment, a relative movement of the test specimen to the sapphire was recorded electrically through a differential transformer. After that, the data conversion from realistic to absolute was made. In **Table 5**, results are summed up, where those of UO_2 are included for comparison [14,15]. It is notable that ref. (14) is from the MATPRO-11 known as rather conservative, while ref. (15) is from the JAERI's design data known as rather realistic.

By figures shown in the table, sensitivity studies for two cases were made. One is addressed to the relationship between $MgAl_2O_4$ and SZR (Zr). As shown in **Fig. 15**, LTE of the inert matrices increased with the increasing temperature. Relatively, the increase of $MgAl_2O_4$ caused the decrease of LTE in magnitude. Another one is, as shown in **Fig. 16**, addressed to relationship of LTE between the simulated ROX fuel and UO_2 [14,15] fuels. Clearly, there is no significant difference between the two.

In conventional PWR, a fuel centerline temperature of UO_2 pellet irradiating at an average linear power of 20 kW/m is to be about 1,000℃, therefore, a magnitude of LTE at this temperature level was chosen for discussion. The LTE of UO_2 fuels at the temperature ranged from 0.87 to 1.1% according table 5. The LTE of ROX fuels ranged from 0.89 to 0.93%. The difference is only 0.2%. Since, it can be said that PCMI to be induced by the thermal expansion of the fuels may be insignificant between the conventional UO_2 fuel and the simulated ROX fuel. The detail discussion on this subject is reported separately [16].

2.5.2 Relocation propensity

During in-core usage, a thermal stress will occur in the simulated ROX fuel, because the fuel composed of many different compounds having different values of LTE. This phenomenon may become important from a viewpoint of fuel dimensional stability, especially in connection with fuel relocation at BOL. Namely, if a pellet is stress-free condition during fabrication stage, a residual stress will be yielded after cool down of the fabricated pellet to room temperature. Conversely, if a pellet is stress-free condition at room temperature, a thermal stress will occur during an in-core usage. A magnitude of thermal stress is estimated as follows. Hence, a thermal stress due to different LTE in different compounds in a ROX matrix can be expressed by [17]

$\sigma_r = -\beta(\gamma_p/\gamma)^3$

$\sigma_\theta = -0.5\beta(\gamma_p/\gamma)^3$

$\beta = (\alpha_m - \alpha_f)\Delta T / [\{(1+\nu_m)/2E_m\} + \{(1-2\nu_f)/E_f\}]$

where ΔT is the temperature difference, σ_r the radial stress, σ_θ the circumferential stress , E the Young's modulus, α the LTE, ν the Poisson's ratio, γ_p the radius of dispersed compound assumed as sphere and γ the radius of spherical matrix including dispersed compound, respectively. Suffix f and m are representing the dispersed compounds and the matrix.

Assuming that dispersed compound and matrix are respectively SZR and $MgAl_2O_4$(spinel), then $\beta = 1.5\times10^{-6}\Delta T / [\{(1+0.247)/2\times257\} + \{(1-2\times0.31)/210\}] = 354\times10^{-3}\Delta T$(MPa) is given. At boundary between dispersed compound and matrix($\gamma_p/\gamma = 1$), a radial stress will be given by $\sigma_r = -\beta(\gamma_p/\gamma)^3 = -354\times10^{-3}\Delta T$(MPa). If matrix of dispersed fuel is only composed of SZR , then σ_r will be given by $-295\times10^{-3}\Delta T$(MPa). The temperature difference between dispersed compound($MgAl_2O_4$) and matrix(SZR) may be very low to the magnitude of ΔT=-373(K). Due to poor data base about a fracture strength of the tested specimens as a function of temperature , it is hard to know whether or not a thermal stress derived from above equations(110-130 MPa at ΔT=-373K) has a potential to cause crack in ROX fuels. It is notable to indicate that the bending strength of sintered MgO at 373(K) is about 180 MPa. It implies that according to calculation a fuel crack by means of residual stress of ROX fuels is impossible to occur at temperature level of ΔT=-373(K) but possible to occur at 1,273(K).

It is worthy of mentioning that the ROX fuel (in this case PuO_2 was contained

instead of UO_2) in form of disk having O.D. by 3mm and t by 1mm was irradiated at 1,000℃ to the burn-up of 20 MWd/kg. It consisted of 23wt%PuO_2-SZR-$MgAl_2O_4$-Al_2O_3 and was fabricated by JAERI similarly to the test specimens used in the present study. Post-irradiation examination (PIE) [18] showed that plate-through and incipient cracks occurred markedly. At design stage, the disk fuel was thought to have no temperature difference across the disk diameter by 3mm. Despite of such intention in the design stage, there occurred two types of cracks in the course of irradiation. Hence, as discussed above the ROX fuel caused cracks during in-core usage. Regarding a resistibility of ROX fuel against thermal shock, a further study may be necessary.

On UO_2 fuel under the usage in LWR, a pellet crack at BOL was known to occur by thermal shock. It was often caused at temperature gradient $\Delta T > 373$(K) across a fuel radius. This was confirmed not only from out-of-pile experiment [19] but also from in-pile experiment [20]. With respect to the simulated ROX fuel, no irradiation tests in form of pellet with cladding were carried out to date. This kind of irradiation test to study a fuel dimensional stability is necessary to perform.

2.6 Creep

During the in-core usage of a ROX fuel, a fuel pellet deforms in the axial and the radial directions with the increase of linear heat generating rate and causes PCMI. Usually the magnitude of PCMI will be reduced by occurrence of creep and stress relaxation. Creep properties of the ROX fuel is therefore one of important matters related to PCMI. Of course, the most interesting is to measure creep rate under irradiation as a function of burn-up, however, here a creep behavior of the simulated ROX fuel under the one-dimensional constant compressive stress is studied.

With an apparatus shown in **Fig. 17**, the test specimen was compressed axially with the constant temperature and the load [10]. Then, the axial displacement of fuel pellet without a radial constraint was obtained as a function of time, hence the obtained was inconstant axial creep rate, differing from a constant axial creep rate really occurring in a core. Results are summed up in **Table 6**. It is clear that the faster the rate of creep, generally safer the fuel from PCMI failure. Obtained inconstant creep rate of the test specimens was dependent on each applied compressive stress and temperature.

(1) Creep in simulated ROX fuel

From a comparison between the simulated ROX fuel of sp.#12 (26wt%UO_2-24wt%SZR-$MgAl_2O_4$) and that of sp.#16 (24wt%UO_2-23wt%SZR-$MgAl_2O_4$) it is understood that inconstant creep rate of the simulated ROX fuel was very sensitive to the original elements included in $MgAl_2O_4$. Hence the increase of Al_2O_3 element in $MgAl_2O_4$ to the magnitude of 20% in weight and the decrease of MgO element to 40% in weight caused the significant reduction of creep rate in the simulated ROX fuel of order of about 80% at temperatures ranged between 1,300 and 1,400℃. A creep property of the simulated ROX fuel was, therefore, influenced much by those elements in $MgAl_2O_4$. The significant reduction of creep rate may be dependent on the magnitude of hardness of Al_2O_3 included. Therefore, volumetric allotments of Al_2O_3 and MgO elements in $MgAl_2O_4$ compound should be taken into consideration from the viewpoint of the fuel creep property.

(2) Comparison with UO_2

A magnitude of creep rate between the simulated ROX fuels and UO_2 or ThO_2 fuels [15] was compared and shown in **Fig. 18**. Regarding the simulated ROX fuels, data points were selected. The comparison is rather rough because the former was derived from inconstant creep rate while the latter two were derived from constant creep rates. As seen from the figure, stress and temperature applied to the present study are fairly low in magnitude than that of UO_2 and relatively low in magnitude than that of ThO_2. This result is strongly influenced by "constant or inconstant" creep rate at temperature around 1,400℃.

As more reliable tool, the concept of "stress index [21]" is introduced. Hence, the stress index is a ratio of deformation rate (h^{-1}) to log (stress (MPa)). Those from simulated ROX fuels (sp.#12 and #13) and UO_2 fuel [21] were plotted together and shown in **Fig. 19**. The stress index between the simulated ROX fuels and the UO_2 fuels at a low stress region was similar in tendency, even though the comparison was made at different level of the temperatures.

A creep rate of the fuels is the essentially important design factor for the in-core behavior, especially relating to PCMI and relaxation. In general, a fuel having low creep rate will tend to cause a strong PCMI at the pellet-to-pellet interface, resulting in the increase of a potential risk for the fuel failure.

2.7 Vicker's hardness (Hv)

The value of Hv of simulated ROX fuels as a function of temperature was

studied. In the study, the equipment as indicated in **Fig. 20** was prepared for measurement, where test temperatures were changed from room to 1,300℃. At the vacuum chamber, a diamond-head was depressed to the surface of test specimens with time span of 15 seconds by a constant load of 9.8N. The average span of diagonal lines of d (mm) at selected temperatures was measured by an optical scope to decide the Hv defined by the relation Hv=0.189F/d, where F is the applied constant load (N). Results were summed up in **Table 7.** Generally, a magnitude of Hv deceased linearly from room temperature up to about 773K. At temperatures between 773K and 1173K, the Hv was almost kept in constant and above the temperatures up to 1,573K it decreased again. It is worthy of mentioning that the magnitude of Hv was changed significantly about the half of MP(1,911℃).

To understand the influence of individual components on the Hv, two from the simulated ROX fuels (sp.#12 and sp.#16) and two from the inert matrices (sp.#2 and sp.#3) were chosen. Result is shown in **Fig. 21.** The Hv tended to decease with the increasing temperature up to 1,300℃. Hence, at temperatures from room to about 500℃, there occurred almost a linear declination. At temperatures between 500 and 900℃, it was nearly constant (like plateau). The end of plateau coincided with the half of the MP. Above 900℃, the Hv decreased again.

(1) Simulated ROX fuels and inert matrices

A comparison between the sp.#2 and the sp.#3 (inert matrices) implied that the decrease of Al_2O_3 in $MgAl_2O_4$, namely the increase of SZR tends to decrease a magnitude of Hv. While, a comparison between the sp.#2 and the sp.#12 led that the Hv of inert matrix was greater in magnitude than that of the simulated ROX fuel. From the viewpoint of hardness as well as creep propensity, a suitable volume of Al_2O_3 in $MgAl_2O_4$ compound should be selected before the fabrication stage.

(2) Comparison with UO_2

Comparing with UO_2 data [22,23], the Hv of simulated ROX fuel as shown in the figure was significantly high in magnitude. At temperatures<500℃, the Hv of simulated ROX fuel was 2-4 times greater than that of UO_2.

2.8 Thermal Diffusivity

2. 8. 1 Measuring method

A thermal diffusivity (hereinafter denoted often as α) is known to be one of key factors in the design applications. It takes an important role not only for studying the transient heat flow of a reactor fuel during accident but also for determination of the safe operating temperature of LWR fuel to prevent from the melting. The flash method [24] has been used to measure α in a wide range of solid materials including UO_2 fuels. It is particularly advantageous because of the simple specimen geometry, small specimen size requirements, rapidity of measurements, and ease of handling materials having a wide range of α values covering large temperature range with a single apparatus. The short measurement times involved reduce the chances of contamination and change of specimen properties due to exposure to high temperature environment [25].

2. 8. 2 Determination of thermal diffusivity

The thermal diffusivity α can be determined either by the half time method ($t^{1/2}$) or by the logarithmic method as described in the below [26]. The two methods broadly belonged to the flash method.

The former is given by $\alpha_h=0.1388\ d^2/t^{1/2}$, where $\alpha_h\{m^2/s\}$ is the thermal diffusivity by half time method , d{m} the specimen thickness at room temperature, $t^{1/2}$ {s} the time required for the back surface of test specimen to reach half of the maximum temperature rise ($0.5\Delta Tm$). In this relation, non-uniform of heating, that is, pulse shape, heat leak from test specimen and thermal expansion of test specimen towards thickness are not taken into consideration.

The latter is given by $\alpha_l = -d^2/4h$, where $\alpha_l\{m^2/s\}$ is the thermal diffusivity by logarithmic method, d{m} the specimen thickness at room temperature, h {s} the gradient of the curve given by $ln\,(t^{1/2} \cdot \Delta T)$ as a function of 1/t , only applicable at the restricted temperature range of $0.3 \leqq \Delta T/\Delta Tm \leqq 0.6$ in temperature history of the heated specimen[27]. It is noted that ΔTm is the maximum temperature rise and ΔT the temperature increment corresponded from a room temperature to a temperature at time t. In this relation, a thermal expansion of test specimen towards thickness is not taken into consideration.

A schematic diagram used for determining both α_h and α_l is shown in **Fig. 22.** In the vacuum chamber, a test specimen with a thickness d was heated uniformly to a certain temperature level prior to the laser beam irradiation injected from the upper surface of the specimen. A transient temperature increase occurred at the

buck surface of specimen was directly monitored through the attached thermocouple combined with two optical systems. Subsequently, obtained data were transferred into the data logging system and transferred to the recorder. The geometry of test specimens used was already shown in table 1, where 8 specimens having different compositions were included. They were in form of the disk shape having diameter from 7.8 mm to 9.4 mm. Thickness was fabricated in the range of 0.7～2.1mm.

Obtained α_h and α_l from the tests are respectively summarized in **Table 8** and **Table 9**. Specimens #12 and #13 were chosen for data comparison between the two methods. The result is shown in **Fig. 23**. The difference occurred by the two methods seems to be small in magnitude at the low temperature regions but relatively high in magnitude at the high temperature ones. It showed that the value obtained from half-time method is larger than that of logarithmic one. A maximum difference between the two was <20% at the high temperature regions. According to the previous study [28], data obtained from the logarithmic method are rather accurate than those from the half-time one. So, in the subsequent discussions, data obtained from the logarithmic method is used.

From Table 9, the thermal diffusivity α_l versus test temperature as a function of fuel compositions is studied. As clear from the table, the measurement was carried out at a certain temperature level in each specimen. In the data plotting, those were represented by 298, 373, 473(K), and so on. This simplification caused the data deviation of $\pm$4K in maximum.

(1) Inert matrices

The α_l of five inert matrices was plotted together and shown in **Fig. 24**. The α_l tended to decrease gradually with the increase of temperature. $MgAl_2O_4$ (sp.#1) showed the highest magnitude of α_l ranging from 0.045 to 0.010 cm^2/s at temperatures studied. On the other hand, SZR (sp.#5) showed the lowest magnitude of α_l as high as 0.006 cm^2/s. Another three fell between the two. As a general trend, the increase of SZR degraded the α_l.

(2) Simulated ROX fuels

Regarding the α_l of simulated ROX fuels, data from the sp.#12 and the sp.#13 were plotted together with those from the sp.#2 and the sp.#3 (references) for a comparison. Obtained is shown in **Fig. 25**. The α_l of simulated ROX fuels was slightly low in magnitude than that of references. This might be attributed to the

existence of UO_2 in the former as heavier elements giving more complicated crystal structures at temperatures <1,000℃. It is also clear that the use of a large volume of SZR as the fissile confinement may degrade α_1 significantly. The degradation makes the simulated ROX fuel hot. In contrast with this, the use of $MgAl_2O_4$ may increase the α_1.

(3) Comparison with UO_2

The α_1 of sp.#12 and sp.#13 was compared to that of UO_2 derived from Owada et al [29]. In the latter, both unirradiated and irradiated UO_2 up to 63GWd/t at Halden Boiling Water Reactor (HBWR, Norway) were used. In the former, the thickness and the weight of each specimen was 1.04mm and 0.2395g. They had outer diameter of 5.28mm and density of 10.52 g/cc. In the latter, the thickness and the weight of the specimens was 0.925mm and 0.1036g, respectively. Between the present study and Owada et al. the measurement tool is the common.

The result is shown in **Fig. 26**. The α_1 of simulated ROX fuels is revealed to be comparable or slightly less in magnitude than that of unirradiated UO_2. The worst value of the α_1 of simulated ROX fuels fell down to data band between the unirradiated and the irradiated UO_2 fuel.

(4) Comparison with UO_2-Gd_2O_3

In LWR, a gadolinia doped UO_2 fuel (UO_2-Gd_2O_3) is using widely for the purpose of reactivity control at an early stage of irradiation. The doping is known to degrade the α_1 of UO_2 fuel. The influence of Gd_2O_3 doping on α_1 of UO_2 was studied by Hirai et al. [30] by means of the logarithmic method. Parameters taken there were the contents of Gd_2O_3 to the amounts of 3, 6 and 10 wt%. In the present paper, the α_1 obtained from 1) pure UO_2 [29], 2) simulate ROX fuel represented by the sp.#12 and 3) Gd_2O_3 doped UO_2 [30] were studied.

They are plotted together in **Fig. 27**. It is revealed that with increase of Gd_2O_3 content the α_1 of Gd_2O_3 doped fuel is decreased to the magnitude of 40% of that of pure UO_2. It is worthy of mentioning that as shown in figure, the α_1 between the simulated ROX fuel (26wt%UO_2-24wt%Zr-$MgAl_2O_4$) and Gd_2O_3 doped UO_2 fuel with content of 10wt% is comparable, or partly high in magnitude in the former.

2.9 Thermal Conductivity

The thermal diffusivity (α) results in many cases can be combined with values for a specific heat (Cp) as well as a density (ρ) and used to derive the thermal

conductivity (λ) by the relation $\lambda = \alpha$ Cp ρ . Dimensions of those are λ {W/m.K}, α {m^2/s}, Cp{J/kg.K} and ρ {kg/m^3}, respectively [31] .

In the present study, the value α of simulated ROX fuels as a function of temperature was obtained from the tests. However, regarding the values of specific heat Cp and density ρ of the simulated ROX fuels, we have no reliable experimental data to date, especially at high temperature>1,000℃.

Matsuda et al [16], however, tried to estimate the specific heat Cp and the density ρ of the simulated ROX fuels. In his study, the lever rule [32] to obtain volume of individual compounds involved in the simulated ROX fuels was used together with the porosity correction factor [33] useful for compensating the density. Separately, Lucuta et al. [34] determined the thermal conductivity of unirradiated UO_2 fuel as similar manner as used by Matsuda et al.

The authors compared the two results and shown in Fig. 28. It is worthy of mentioning that the density ρ of simulated ROX fuels was of order of 47-52% of that of UO_2 (10.41g/cc), however the α_1 of those was comparable or less in magnitude to that of UO_2. The specific heat Cp estimated by Matsuda et al. was about two times greater than that of UO_2. As a result, the thermal conductivity between UO_2 and the simulated ROX fuel is fell into comparable. It is found from the present study that the increase of SZR causes either the decrease of α_1 (see, Fig. 24) or the increase of density ρ (see, Fig. 3). The two were factors of the thermal conductivity as given by above relation. It is revealed from Fig. 28 that the increase of SZR from 24wt% to 43wt% degrades the thermal conductivity of order of about 30%. This fact implies that within this experimental condition the increase of SZR rather affected with degradation of the α_1 .

3. Concluding Remarks

Out-of-pile tests in order to know the physical characteristics of simulated rock-like oxide (ROX) fuels were carried out. The followings were revealed.

(1) From the X-ray diffraction study it was revealed that a) UO_2 could be dissolved into SZR matrix and b) $MgAl_2O_4$ (spinel) was produced alone when Al_2O_3 powder was mixed with MgO powder with the condition of $Al_2O_3 \geqq MgO$. The technique to fabricate the simulated ROX fuel (UO_2-SZR-$MgAl_2O_4$) was successfully built up.

(2) The GID of simulated ROX fuels ranged from 4.9 to 5.4g/cc, they were of order of about 47-52% of GID of UO_2. The GID between the core (UO_2 and SZR) of simulated ROX fuel and the inert matrix ($MgAl_2O_4$ (spinel)) was compared. The GID of the former is greater than that of the latter to the magnitude of 30%. The increase of SZR makes the simulated ROX fuel dense to the magnitude of 60%, while that of $MgAl_2O_4$ makes the simulated ROX fuel coarse to the magnitude of about 30%.

(3) The melting point of simulated ROX fuels was 1,911±39℃, about 30% lower than that of UO_2 .

(4) The values of LTE between the simulated ROX fuel and UO_2 showed little difference. The value at 1,000℃ was 0.896% for the former and 0.983% for the latter. The LTE was increased with the increased amount of SZR.

(5) The creep rate of simulated ROX fuels was found to be very sensitive to the original elements contained in $MgAl_2O_4$ compound. Namely, the increase of Al_2O_3 of order of 20wt% reduced the creep rate of simulated ROX fuels of order of about 80% at the temperatures between 1,300 and 1,400℃. The creep compared by using the stress index (the ratio of deformation rate to *log* (stress)) showed the similar propensity between the simulated ROX fuel and the UO_2 one.

(6) The Hv became significantly small at temperatures below the half of MP. The tendency was influenced by Al_2O_3 contained in the $MgAl_2O_4$, hence the increase of Al_2O_3 made the simulated ROX fuel mor hard. The Hv of simulated ROX fuel is larger than that of UO_2 to the factor of 2-4.

(7) The α_1 became greatest in $MgAl_2O_4$ having the magnitude from 0.045 to 0.010 cm^2/s. In the inert matrices, the α_1 was degraded gradually with the increase of SZR due to a poor thermal conductivity of 0.006 cm^2/s in SZR up to temperatures< 1,400℃. The difference in α_1 between the simulated ROX fuels and the unirradiated UO_2 fuels was not so significant. Similarly, the difference in α_1 between the simulated ROX fuels and the Gd_2O_3-doped UO_2 fuels up to 10wt% was also little.

(8) The magnitude in thermal conductivity between the simulated ROX fuel and the UO_2 fuel is comparable. Degradation occurred by the increase of SZR.

(9) Within this experimental scope, the sp.#12 consisted of 26wt%UO_2-24wt%Zr-50wt%$MgAl_2O_4$ is seemed to be most feasible for future studies.

4. Afterword

Differing from UO_2 having a single-phase structure, the ROX fuel developing in JAERI has to have at least three different major compounds such as PuO_2, SZR and $MgAl_2O_4$. These multi-compound structures put the ROX fuel very complicated situation. To increase the reliability of ROX fuels a lot of SZR as a UO_2 container is needed. Increased use of the SZR, however, tends to degrade the thermal diffusivity and makes the ROX fuel hot during in-core usage.

To compensate this minority, the use of $MgAl_2O_4$ is taken into consideration. The use of $MgAl_2O_4$ is found to be effective to increase the thermal diffusivity, however, the creep property became worse. Degradation of the creep propensity will lead the occurrence of hard PCMI during an in-core usage. Further, the $MgAl_2O_4$ made decrease of the fuel bulk density and the reduction of Hv significantly. The potential risk from the former is to cause the greater densification at the BOL and greater swelling at the end-of-life. The potential risk from the latter is to cause the degradation of gap conductance between ROX pellet and cladding. It will make the ROX fuel hot. More simply to say that the use of SZR tends to degrade the thermal property of ROX fuel, while the use of $MgAl_2O_4$ tends to degrade the mechanical property of the ROX fuel, respectively. From this point of view, the components of ROX fuel should be balanced well at the stage of fabrication.

More attention must be paid on the fact that the MP of ROX fuel (1,911℃) is about 30% lower than that of UO_2. The low MP of the ROX fuel compared with UO_2 is inevitable due to its multi-component phases.

Obtained data from the present study should be useful for characterizing the ROX fuel from the viewpoint of computer code modeling. Regarding a UO_2 fuel in LWR, one of the authors developed the steady-state/transient fuel behavior computer code FPRETAIN[5]. Data from the present study is believed to be useful for modifying the computer code for the ROX fuel.

Acknowledgment

The authors wish to thank Mr. S. Kobayashi, Engineer of Nuclear Fuel Industries, Ltd., for his valuable comments. Grateful acknowledgment is addressed to Mr. I. Owada, Department of Hot Laboratories, JAERI for his technical comments made with respect to the laser flash method and to Mr. M.

Fujita, Department of Reactor Safety Research, JAERI for his fruitful suggestions during data comparison between UO_2 fuel and ROX one.

References

(1) At. Energy Commission: " *Long-Term Program for Research Development and Utilization of Nuclear Energy*",(1994), [in Japanese].

(2) Oi, N.: "*Plutonium challenges-Changing dimensions of global cooperation*", IAEA Bulletin, vol.40, {1}, p12 (1998).

(3) Muromura, T., Nitani, N., Akie, H., Takano, H.: "Plutonium Rock-like Fuel Integrated R&D (PROFIT) ", *IAEA-TCM, Unconventional Options for Plutonium Disposition,* Obninsk, Russia, 11/7-11, (1994).

(4) Kimura, H., Matsuzuru, H., Takano, H., Muromura, T. : " Environmental Safety of the Geologic Disposal of ROX and MOX Spent Fuels", JAERI-Research 97-049 (1997), [in Japanese].

(5) Yanagisawa, K., Ichikawa, M., Saito, H. : " Simulations by Computer Codes FEMAXI-III and FPRETAIN for In-core Behavior of LWR Fuel ", *Proc. Int., Conference. on Supercomputing in Nuclear Applications*, p.131, BS081, Mito City, Japan (1990).

(6) Levin, E. M., McMurdie H. F., Hall, F. P.: " Phase Diagram for Ceramists", The American Ceramic Society Inc., (1956).

(7) Yanagisawa, K., Hayashi, K. : " In-pile Densification of UO_2 Pellet Irradiated up to 1,720 MWd/tU", *J. Nucl. Mater.*, 127, 116 (1985).

(8) Yanagisawa, K.: " Grain Size, Porosity and Pore Distribution Measurement of UO_2 Fuel by Image Analyzer Apparatus (QTM)", JAERI-M 7289 (1977), [in Japanese].

(9) Mizushima, M., et al: *Encyclopaedia Chimica*, Kyoritsu Shuppan, Vol.1-10 (1960), [in Japanese].

(10) Watarumi, K., Kawanishi, K.: *Ann. Mtg., At. Energy Soc., Jpn,* G36,(1988), [in Japanese].

(11) Yamanouchi, S., Tachibana, T., Tsukui, K., Oguma, M.: "Melting Temperature of Irradiated UO_2 and UO_2-2wt% Gd_2O_3 Fuel Pellets up to Burnup of about 30GWd/tU", *J. Nucl. Sci. Technol.*, 25[6], 528(1988).

(12) Yamada, T., Yoshimura, M., Somiya, S.: " Redetermination of the solidification points of Al_2O_3, Y_2O_3, and HfO_2 by digital pyrometry with an arc-imaging furnace ", *High-Temperature-High Pressures*, 18, 377(1986).

(13) Furuya, H., Muraoka, S., Muraoka, T. : " Feasibility of Rock-like fuel and glass waste form for disposal of weapons plutonium", *NATO Advanced*

Research Workshop, " Disposal of Weapons Plutonium-Approaches and Prospects", 14-17May 1995, St. Petersburg, Russia (1995).

(14) MATPRO-Version 11, " A Handbook of Materials Properties for Use in the Analysis of Light Water Reactor Fuel Rod Behavior", Idaho National Eng., Lab. (1981).

(15) Morishima, A., Kuriyama, M., Harayama, Y., Shiratori, T., Izumi, F., Fujita, M. : " Design for Power Reactor Fuel Assemblies", JAERI-M 4881 (1972), [in Japanese].

(16) Matsuda, T., Kobayashi, S., Shirasu, N., Yamashita, T., Ohmichi, T., Muromura, T.: " Thermal Expansion and Thermal Conductivity of Rock-like Fuel", JAERI-Research 97-083, (1997), [in Japanese].

(17) Selsing, J. : *J. Am. Ceramic. Soc.*, **44**, p.419 (1961).

(18) Yanagisawa, K., Ohmichi, T., Kanazawa, H., Amano, H., Yamahara, T : " Fission Gas Release from Rock-like Fuels, PuO_2-ZrO_2(Y){or ThO_2}-Al_2O_3-MgO at Burn-up of 20MWd/kg ", JAERI-Research 97-085 (1997).

(19) Oguma, M. : "Integrity Degradation of UO2 Pellets Subjected to Thermal Shock ", *J. Nucl. Mater.,* 127, 67(1985).

(20) Turnbull, J. A., Appelhans, A.D. : "Fuel Behaviour Irradiated from Internal Gas Flow and Temperature Measurements Made at the Beginning-Of-Life of IFA-504", *Proc. Enlarged Halden Programme Group Mtg.*, Hanko, Norway (1981).

(21) Kingery, W.D., Bowen, H.K., Uhimann, D.R.: Introduction to Ceramics, 2nd edition, John Wiley &Sons, p.752 (1976).

(22) Kim, S., Takagi, O., Obata, N., Kirihara, T.: *J. At. Energy Soc. Jpn*, 25[2], 140(1983), [in Japanese].

(23) Walker, W. W.: *The Science. of Hardness Testing and Its Research Application.,* 258(1973).

(24) Parker, W. J., Jenkins, R. J., Butler, C. P., Abbott, G. L. : " Flash Method of Determining Thermal Diffusivity, Heat Capacity, and Thermal Conductivity", *J. Applied Physics,* 32(9), 1679 (1961).

(25) ASTM: E 1461-92: " Standard Test Method for Thermal Diffusivity of Solids by the Flash Method", (1992).

(26) Azumi, T., Takahashi, Y. : " Novel Finite Pulse-Width Correction in Flash Thermal Diffusivity Measurement", *Rev. Sci. Instrum.*, 152(9), 1411 (1981).

(27) Azumi, T., Takahashi, Y., Kanno, M.: *Proc. 2nd Japan Thermal Property Symposium*, 19 (1981).

(28) Takahashi, Y., Yamamoto, K., Ohsato, T.: " Advantages of Logarithmic

Method-A New Method for Determining Thermal Diffusivity-in the Laser Flash Technique", Netsu Sokutei, 15(3), 103 (1988).

(29) Owada, I., Nishino, Y., Yamahara, T., Ishimoto, K.: " Development of Remote Handling Apparatus for Measuring Thermal Diffusivity", *Proc. 43rd Conf. On Robotics and Remote Systems*, pp75 (1995).

(30) Hirai, M.: "Thermal diffusivity of UO_2-Gd_2O_3 pellets", *J. Nucl., Mater.*, **173**, 247(1990).

(31) JIS R1611: " Testing methods of thermal diffusivity, specific heat capacity, and thermal conductivity for high performance ceramics by Laser Flash method", (1991).

(32) The Society of Calorimetry and Thermal Analysis, Japan: "MALT 2", Kagaku Gijitsu-sha, Tokyo, Japan, (1992), [in Japanese].

(33) Loeb, A. L. : *J. Am. Ceramic. Soc.*, **37**, 96 (1954).

(34) Lucuta, P. G., *et al:* "Thermal conductivity of SIMFUEL", *J. Nucl., Mater.*, **188**, 198(1992).

Table 1 Characterization of simulated ROX fuel used

Spec. No.	Element(wt%)[1] SZR[4]	Al_2O_3	MgO	UO_2	Geometrical[2] Density(g/cc)	Outer Diameter(mm)	Length (mm)	L/D	t[3] (mm)
#01	-	72(50)	28(50)	-	3.21±0.08	7.790±0.050[5]	9.176±0.541	1.18	0.741
#02	32(20)	49(40)	19(40)	-	3.96±0.02	9.165±0.008	9.880±0.321	1.08	2.038
#03	56(40)	32(30)	12(30)	-	4.47±0.04	9.133±0.009	9.944±0.678	1.09	2.082
#04	88(80)	8(10)	4(10)	-	5.12±0.01	9.278±0.006	10.354±0.058	1.12	2.078
#05	100(100)	-	-	-	5.19±0.02	9.385±0.007	9.778±0.618	1.04	1.113
#06	30(20)	57(50)	13(30)	-	2.89[6]	9.994±0.039	8.042±0.004	0.80	-
#12	24(18)	36(36)	14(36)	26(10)	4.74±0.07	8.937±0.007	10.178±0.203	1.14	1.979
#13	43(36)	24(27)	9(27)	24(10)	5.07±0.01	9.182±0.004	9.022±1.780	0.98	2.024
#16	23(18)	43(45)	10(27)	24(10)	4.77±0.01	8.850±0.004	10.149±0.445	1.15	2.020

Note:(1) Parenthesis means corresponded molecular percent at in form of powder.
(2) Geometrical density after sintering at 1750℃/4h with N_2+$3H_2$ environment
(3) Thickness provided thermal diffusivity measurement.
(4) SZR: Stabilized zirconium dioxide (ZrO_2) in form of 88.8mol%ZrO_2-11mol%Y_2O_3-0.2mol%Gd_2O_3.
(5) In common, the fuel pellets were flat without center hole. Grain size was about 10 μ m.
(6) This data has no statistical error band due to one time measurement. For others, 3 to 14 samples derived from the same lot were provided for repeated measurements.

Table 2 Results of X- ray diffraction and density measurement

Spec. No.	Compound(wt%) SZR	$MgAl_2O_4$	UO_2	Geometrical Density(g/cc)	He gas immersed[1] Density(g/cc)	Pores[2] Remained(%)	XRD[3]
#01	-	100	-	3.21±0.08	3.52	8.9	S
#02	32	68	-	3.96±0.02	4.09	3.4	S, F
#03	56	44	-	4.47±0.04	4.60	2.7	S, F
#04	88	12	-	5.12±0.01	5.49	6.7	S, F
#05	100	-	-	5.19±0.02	5.89	11.9	F
#06	30	70	-	2.89	4.02	28.1	S, F
#12	24	50	26	4.74±0.07	4.91	3.4	S, F
#13	43	33	24	5.07±0.01	5.37	5.7	S, F
#16	23	53	24	4.77±0.01	4.85	1.8	S, F

Note:(1) Bulk density after immersion into pressurized helium gas.
(2) Pores (%)={1-(geometrical density/He immersed density)}x100.
(3) Phase revealed by X-ray diffraction (XRD), where symbol S represents $MgAl_2O_4$ spinel phase and F does fluorite phase including both SZR and UO_2.

Table 3 Volumetric percentage of compounds

Spec. No.	Compounds (vol.%) UO_2 and SZR	$MgAl_2O_4$
#01	0	100
#02	22	78
#03	43	57
#04	82	18
#05	100	0
#06	20	80
#12	30	70
#13	49	51
#16	28	72

Table 4 Results on MP measurement

Specimen No.	Compounds(wt%) UO_2	SZR	$MgAl_2O_4$	Geometrical[(1)] Density(g/cc)	Melting [(2)] point(℃)
#01	0	0	100	3.21	2,102±0
#02	0	32	68	3.96	1,931±5
#03	0	56	44	4.47	1,929±8
#04	0	88	12	5.12	No data
#05	100	0	0	5.19	2,724±6
#06	0	30	70	2.89	1,864±2
#12	26	24	40	4.74	1,933±10
#13	24	43	33	5.07	1,933±5
#16	24	23	53	4.77	1,866±15

Note:(1) Geometrical density, GD measured after sintering at 1750℃/4h with N_2+$3H_2$ environment

(2) Melting point, MP measured by thermal arrest method. Specimen #04 was not for measurement. MP was calibrated by the method described in the text.

Table 5 Results on measurement of LTE (unit: %)

Spec.	#01	#02	#03	#04	#05	#06	#12	#13	#16	UO_2[Ref.16]	UO_2[Ref.15]
100℃	0.039	0.045	0.045	0.046	0.045	0.043	0.028	0.041	0.046	0.060	0.073
200	0.114	0.124	0.130	0.132	0.134	0.118	0.110	0.124	0.123	0.127	0.173
300	0.193	0.206	0.216	0.221	0.225	0.196	0.195	0.210	0.204	0.200	0.274
400	0.277	0.292	0.304	0.314	0.318	0.278	0.285	0.300	0.289	0.278	0.376
500	0.363	0.382	0.394	0.410	0.416	0.363	0.378	0.394	0.378	0.362	0.479
600	0.452	0.474	0.489	0.510	0.518	0.451	0.475	0.493	0.471	0.452	0.586
700	0.543	0.570	0.587	0.613	0.624	0.544	0.574	0.596	0.568	0.548	0.697
800	0.637	0.668	0.688	0.722	0.736	0.40	0.676	0.703	0.670	0.649	0.811
900	0.732	0.768	0.794	0.835	0.853	0.739	0.780	0.814	0.775	0.756	0.930
1000	0.829	0.870	0.903	0.952	0.974	0.842	0.885	0.927	0.882	0.870	1.052
1100	0.928	0.973	1.013	1.074	1.099	0.948	0.992	1.041	0.993	0.988	1.178
1200	1.029	1.077	1.125	1.199	1.227	1.056	1.100	1.157	1.105	1.113	1.307
1300	1.134	1.180	1.237	1.325	1.357	1.167	1.207	1.273	1.217	1.244	1.440
1400	1.242	1.283	1.347	1.452	1.487	1.280	1.314	1.388	1.330	1.380	1.575
1500	1.354	1.383	1.452	1.574	1.617	1.393	1.421	1.502	1.440	1.522	1.712

Table 6 Results of creep test

Specimen No.	Compounds(wt%) UO_2	SZR	$MgAl_2O_4$		Temperature(℃) 1,300	1,300	1,300	1,350	1,400
					Stress(MPa) 30	40	50	30	30
					Creep rate(h^{-1})				
#02	0	32	68	-	1.95×10^{-3}	2.73×10^{-3}	3.94×10^{-3}	5.96×10^{-3}	26.8×10^{-3}
#03	0	56	44	-	2.50×10^{-3}	4.83×10^{-3}	8.52×10^{-3}	11.1×10^{-3}	41.8×10^{-3}
#12	26	24	50		1.57×10^{-3}	5.61×10^{-3}	7.93×10^{-3}	9.57×10^{-3}	40.3×10^{-3}
#16	24	23	53		0.49×10^{-3}	0.68×10^{-3}	0.93×10^{-3}	1.66×10^{-3}	7.08×10^{-3}

Table 7 Results of Hv test

Temp. (℃)	Specimen#02[1]	Specimen#03	Specimen#12	Specimen#16
25	1,385±53[2]	1,287±78	1,364±46	1,473±94
100	1,275±56	1,179±40	1,178±83	1,306±57
200	1,189±49	1,057±29	1,073±45	1,134±45
300	1,083±31	956±13	883±23	1,008±19
400	938±16	737±49	721±21	925±23
500	847±24	684±19	592±38	855±15
600	792±35	610±17	586±3	794±12
700	798±6	557±29	564±25	783±26
800	744±32	525±18	531±35	768±25
900	744±19	556±13	495±21	715±41
1,000	680±17	534±12	484±11	637±6
1,100	613±21	472±7	426±26	524±13
1,200	497±20	390±6	311±13	384±6
1,300	353±13	286±10	267±9	266±6

Note: (1) Specimen

	Compounds (wt%)		
	UO_2	SZR	$MgAl_2O_4$
#02	0	32	68
#03	0	56	44
#12	26	24	50
#16	24	23	53

(2) Statistical error band obtained from measurements repeatedly

Table 8 Thermal diffusivity of α_{ℓ} determined by half-time method

Specimen #1		Specimen #2		Specimen #3		Specimen #4	
Temp. (K)	α (cm2/s)	Temp. (K)	α (cm2/s)	Temp. (K)	α (cm2/s)	Temp. (K)	α (cm2/s)
296	0.0440	300	0.0395	299	0.0261	301	0.0102
371	0.0336	371	0.0321	373	0.0225	372	0.0091
469	0.0262	470	0.0250	472	0.0173	471	0.0084
571	0.0215	571	0.0196	572	0.0149	571	0.0079
673	0.0185	673	0.0170	672	0.0133	673	0.0076
772	0.0167	772	0.0153	770	0.0123	772	0.0073
870	0.0145	870	0.0139	871	0.0112	871	0.0069
975	0.0133	969	0.0128	974	0.0105	974	0.0070
1,073	0.0124	1,070	0.0119	1,073	0.0099	1,072	0.0068
1,174	0.0117	1,172	0.0112	1,172	0.0094	1,172	0.0069
1,271	0.0110	1,269	0.0107	1,274	0.0092	1,271	0.0069
1,375	0.0103	1,372	0.0101	1,370	0.0088	1,372	0.0070
1,473	0.0098	1,471	0.0096	1,473	0.0085	1,470	0.0066
1,571	0.0094	1,572	0.0096	1,572	0.0085	1,571	0.0067
1,672	0.0092	1,670	0.0095	1,672	0.0084	1,669	0.0069

Specimen #5		Specimen #12		Specimen #13		Specimen #16	
Temp. (K)	α (cm2/s)	Temp. (K)	α (cm2/s)	Temp. (K)	α (cm2/s)	Temp. (K)	α (cm2/s)
299	0.0062	297	0.0332	298	0.0252	299	0.0266
375	0.0059	374	0.0264	374	0.0197	374	0.0208
472	0.0056	472	0.0219	473	0.0162	471	0.0174
571	0.0054	571	0.0174	572	0.0143	571	0.0148
673	0.0052	670	0.0154	673	0.0130	671	0.0133
770	0.0051	769	0.0139	771	0.0121	769	0.0122
871	0.0051	872	0.0129	870	0.0114	871	0.0115
971	0.0050	970	0.0117	974	0.0098	974	0.0108
1,072	0.0051	1,071	0.0110	1,073	0.0089	1,072	0.0103
1,173	0.0051	1,173	0.0102	1,173	0.0086	1,174	0.0095
1,273	0.0052	1,272	0.0099	1,272	0.0085	1,272	0.0094
1,371	0.0050	1,374	0.0097	1,373	0.0077	1,372	0.0092
1,472	0.0050	1,470	0.0096	1,471	0.0083	1,473	0.0091
1,571	0.0054	1,570	0.0095	1,572	0.0081	1,572	0.0089
1,671	0.0056	1,672	0.0096	1,671	0.0081	1,672	0.0089

Table 9 Thermal diffusivity of α_{ℓ} determined by logarithmic method

Specimen #1		Specimen#2		Specimen#3		Specimen#4	
Temp. (K)	α (cm2/s)	Temp. (K)	α (cm2/s)	Temp. (K)	α (cm2/s)	Temp. (K)	α (cm2/s)
296	0.0448	300	0.0407	299	0.0260	301	0.0099
370	0.0357	371	0.0332	373	0.0217	372	0.0095
469	0.0281	470	0.0250	472	0.0177	471	0.0088
571	0.0223	570	0.0201	572	0.0151	570	0.0080
672	0.0192	672	0.0172	672	0.0133	673	0.0074
772	0.0173	772	0.0152	770	0.0119	772	0.0072
870	0.0160	870	0.0138	871	0.0115	871	0.0070
975	0.0141	969	0.0126	973	0.0105	974	0.0067
1,073	0.0134	1,070	0.0115	1,073	0.0097	1,072	0.0067
1,174	0.0124	1,172	0.0108	1,172	0.0092	1,172	0.0066
1,270	0.0112	1,268	0.0101	1,274	0.0084	1,271	0.0064
1,374	0.0103	1,372	0.0099	1,370	0.0079	1,372	0.0067
1,473	0.0099	1,471	0.0100	1,473	0.0080	1,470	0.0063
1,571	0.0096	1,571	0.0094	1,572	0.0080	1,571	0.0062
1,672	0.0096	1,670	0.0091	1,672	0.0076	1,669	0.0063

Specimen #5		Specimen#12		Specimen#13		Specimen#16	
Temp. (K)	α (cm2/s)	Temp. (K)	α (cm2/s)	Temp. (K)	α (cm2/s)	Temp. (K)	α (cm2/s)
299	0.0064	297	0.0341	297	0.0250	299	0.0271
374	0.0061	373	0.0266	374	0.0206	374	0.0222
471	0.0058	472	0.0211	472	0.0166	471	0.0184
571	0.0055	571	0.0177	571	0.0144	571	0.0153
673	0.0053	670	0.0153	672	0.0131	671	0.0132
770	0.0052	769	0.0136	771	0.0120	769	0.0121
871	0.0049	872	0.0123	870	0.0113	871	0.0111
971	0.0049	970	0.0115	974	0.0095	974	0.0104
1,072	0.0050	1,071	0.0104	1,073	0.0091	1,072	0.0101
1,173	0.0048	1,173	0.0096	1,173	0.0084	1,174	0.0091
1,273	0.0049	1,272	0.0090	1,272	0.0079	1,272	0.0088
1,371	0.0044	1,374	0.0089	1,373	0.0079	1,372	0.0086
1,472	0.0047	1,470	0.0083	1,471	0.0078	1,473	0.0082
1,571	0.0051	1,570	0.0084	1,572	0.0075	1,572	0.0079
1,671	0.0057	1,672	0.0082	1,670	0.0068	1,671	0.0077

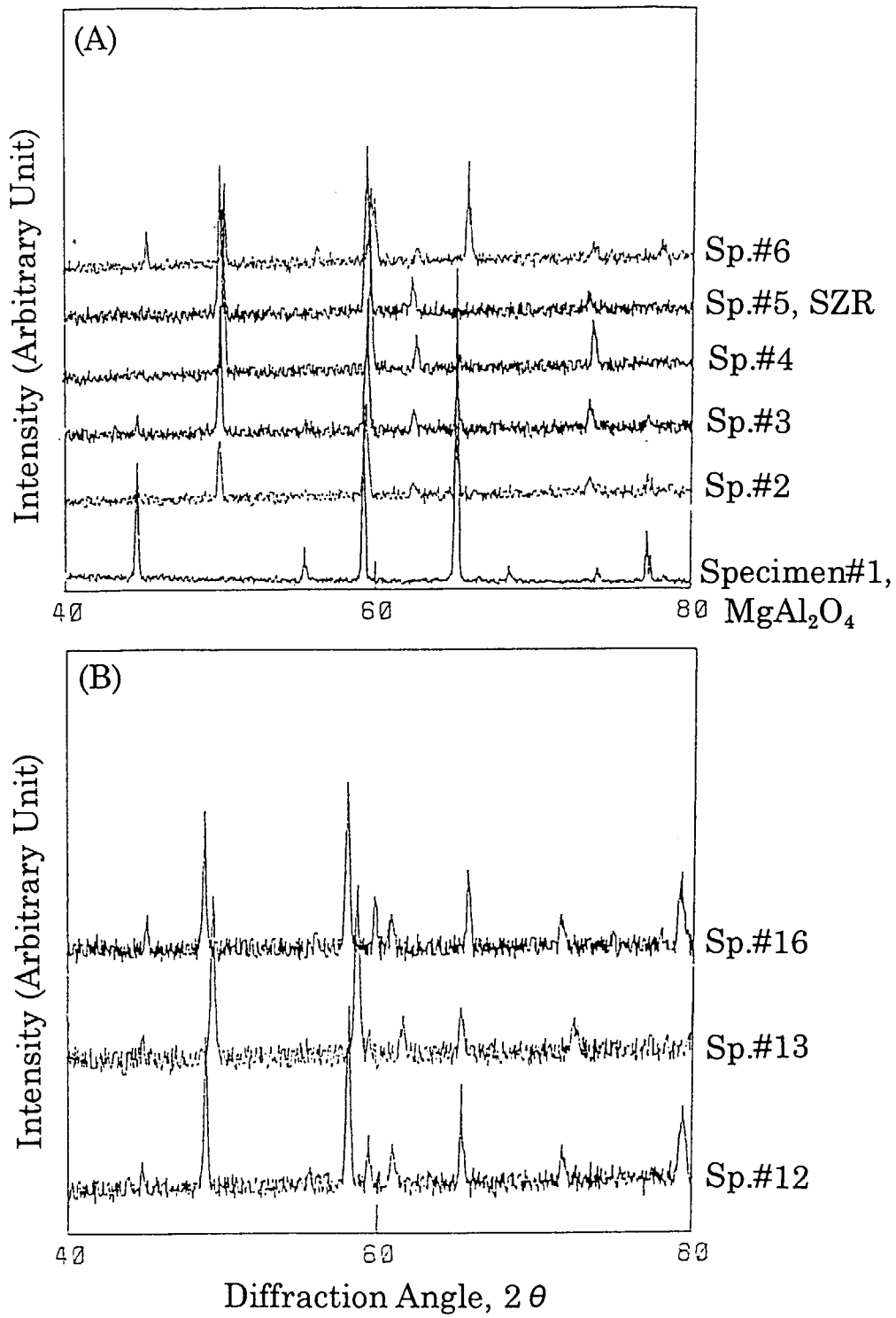

Fig. 1 X-ray diffraction patterns of all test specimens used.
(A) Inert matrices: 100wt%$MgAl_2O_4$(spinel, Sp.#1), 100wt%SZR (Sp.#5) and $MgAl_2O_4$-SZR (Sp.#2, 3, 4 & 6)
(B) Simulated ROX fuels: UO_2-SZR-$MgAl_2O_4$ (Sp.#12,13 &16)

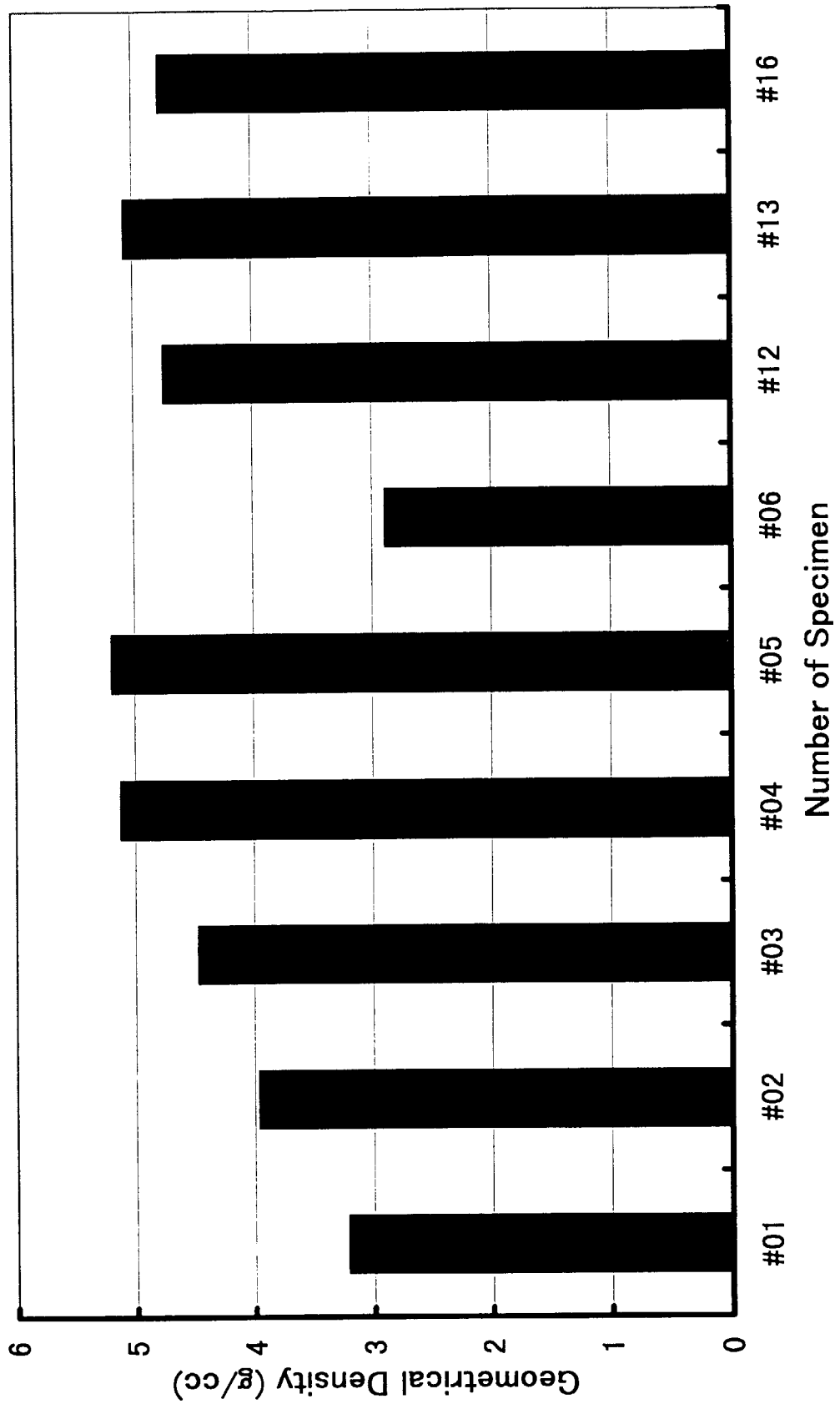

Fig. 2 GD of simulated ROX fuels: sp.#1 and sp.#5 are respectively containing $MgAl_2O_4$ and SZR. Specimens #2, #3, #4 and #6 are mixture of $MgAl_2O_4$ with SZR excluding UO_2. Specimens #12, #13 and #16 are simulated ROX fuels containing UO_2-SZR as fuel core and $MgAl_2O_4$ as inert matrix.

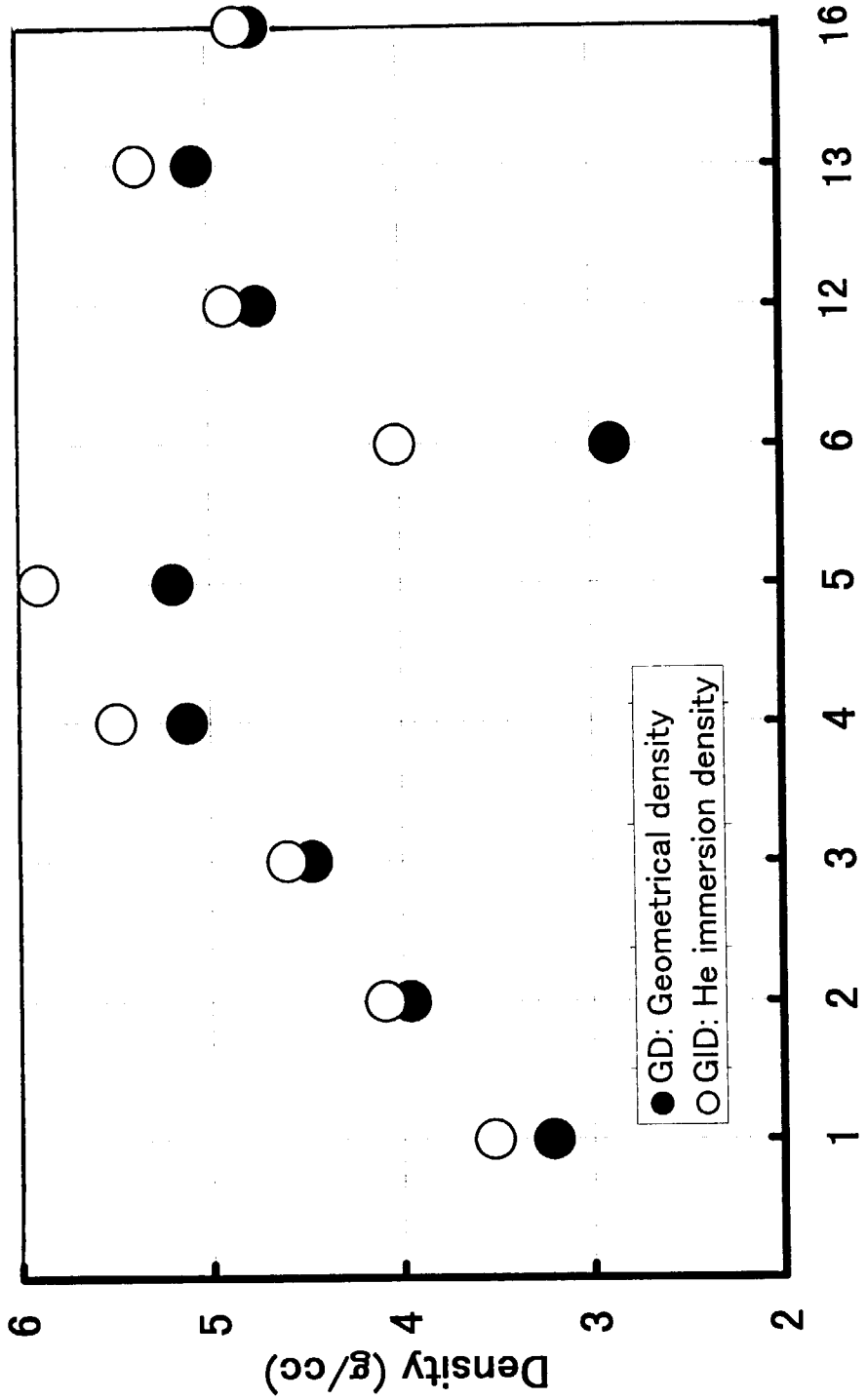

Fig. 3 Relationship between GD and GID

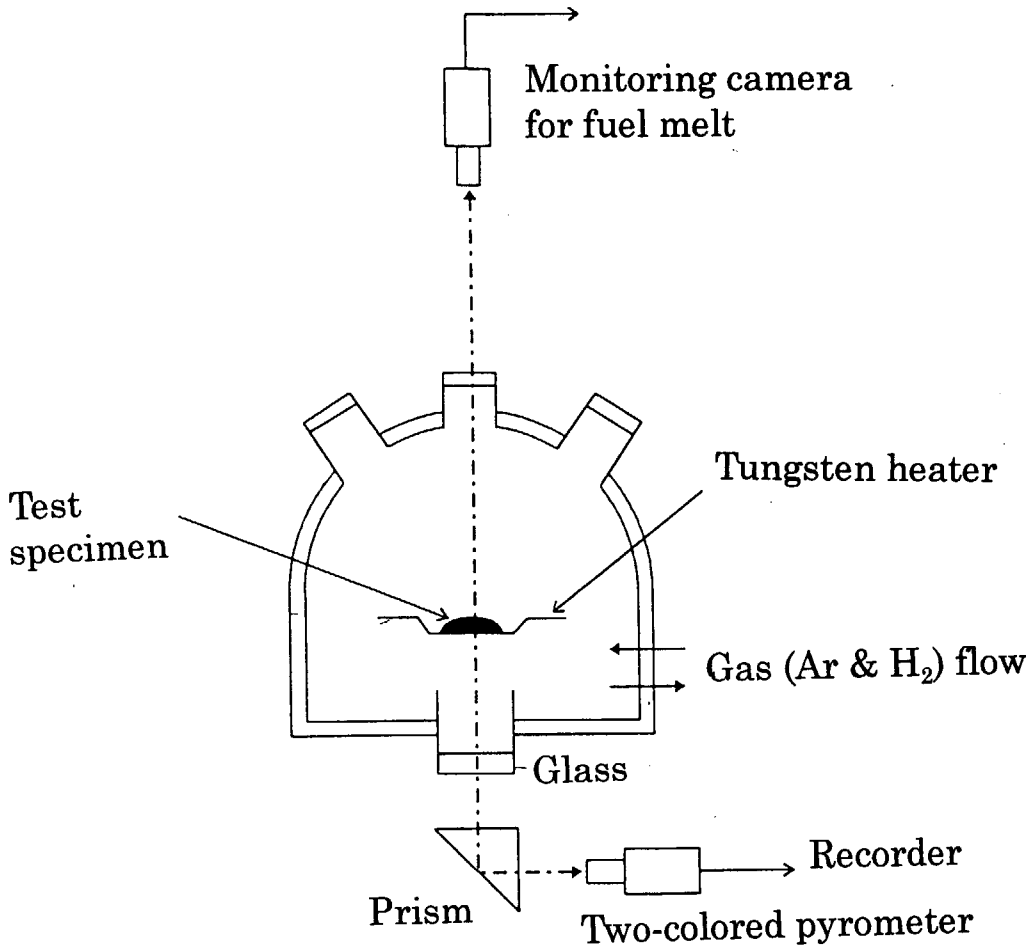

Fig. 4 Apparatus for measurement of MP

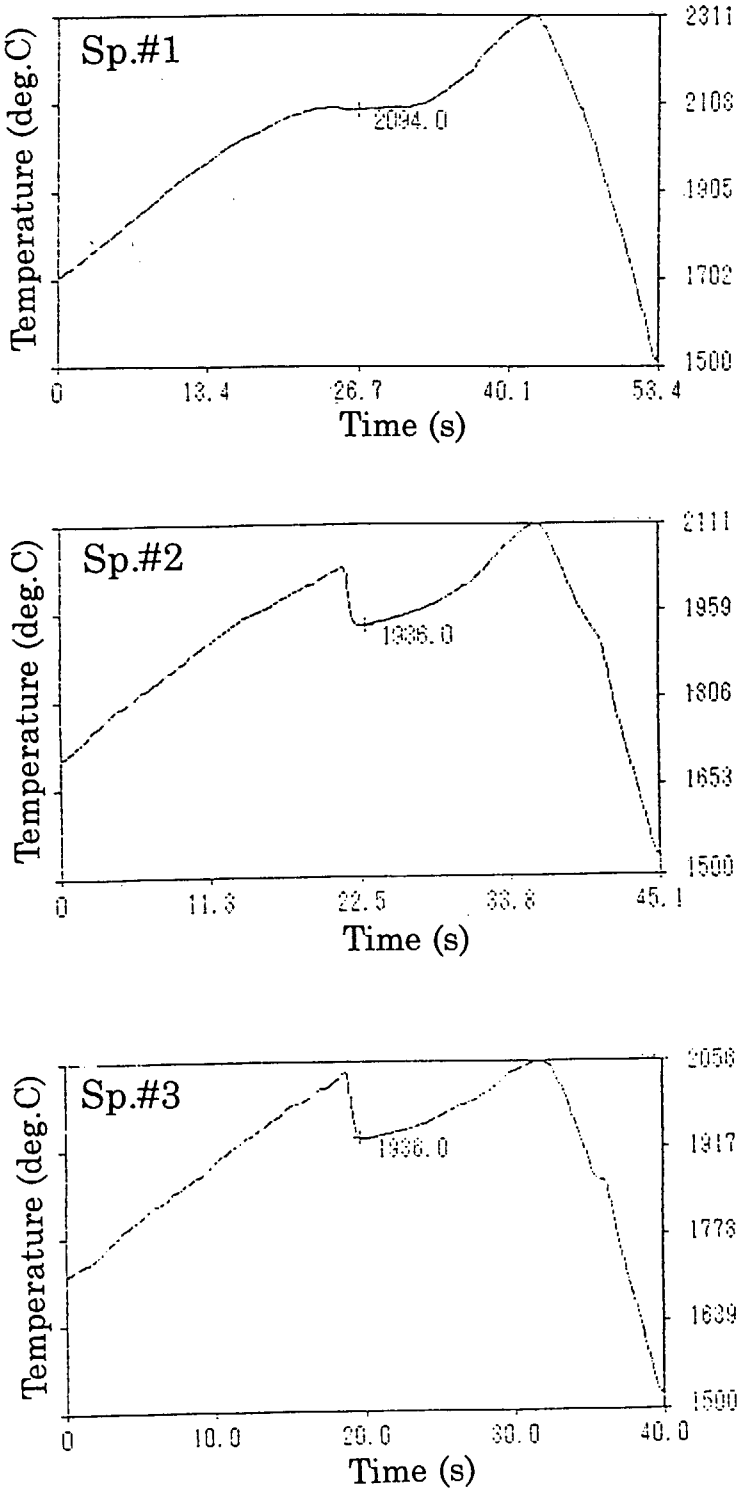

Fig. 5 Typical temperature histories of sp.#1, #2 and #3 obtained from MPmeasurement.
Sp.#1; 100wt% $MgAl_2O_4$,
Sp.#2; 32wt%SZR-$MgAl_2O_4$
Sp.#3; 56wt%SZR-$MgAl_2O_4$

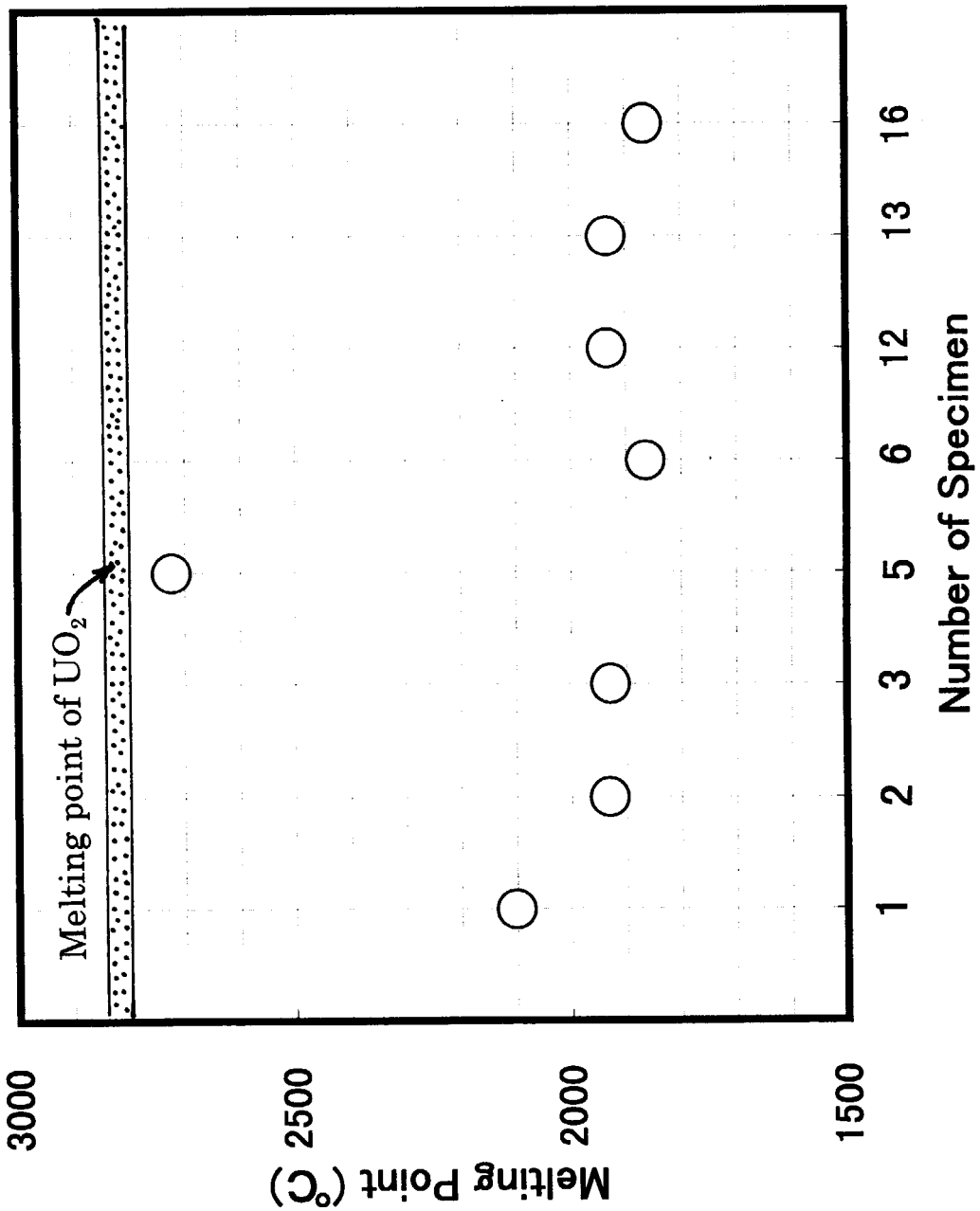

Fig. 6 MP of test specimens used, where sp. #12, #13 and #16 are simulated ROX fuels. MP of UO_2 is indicated by hatched area

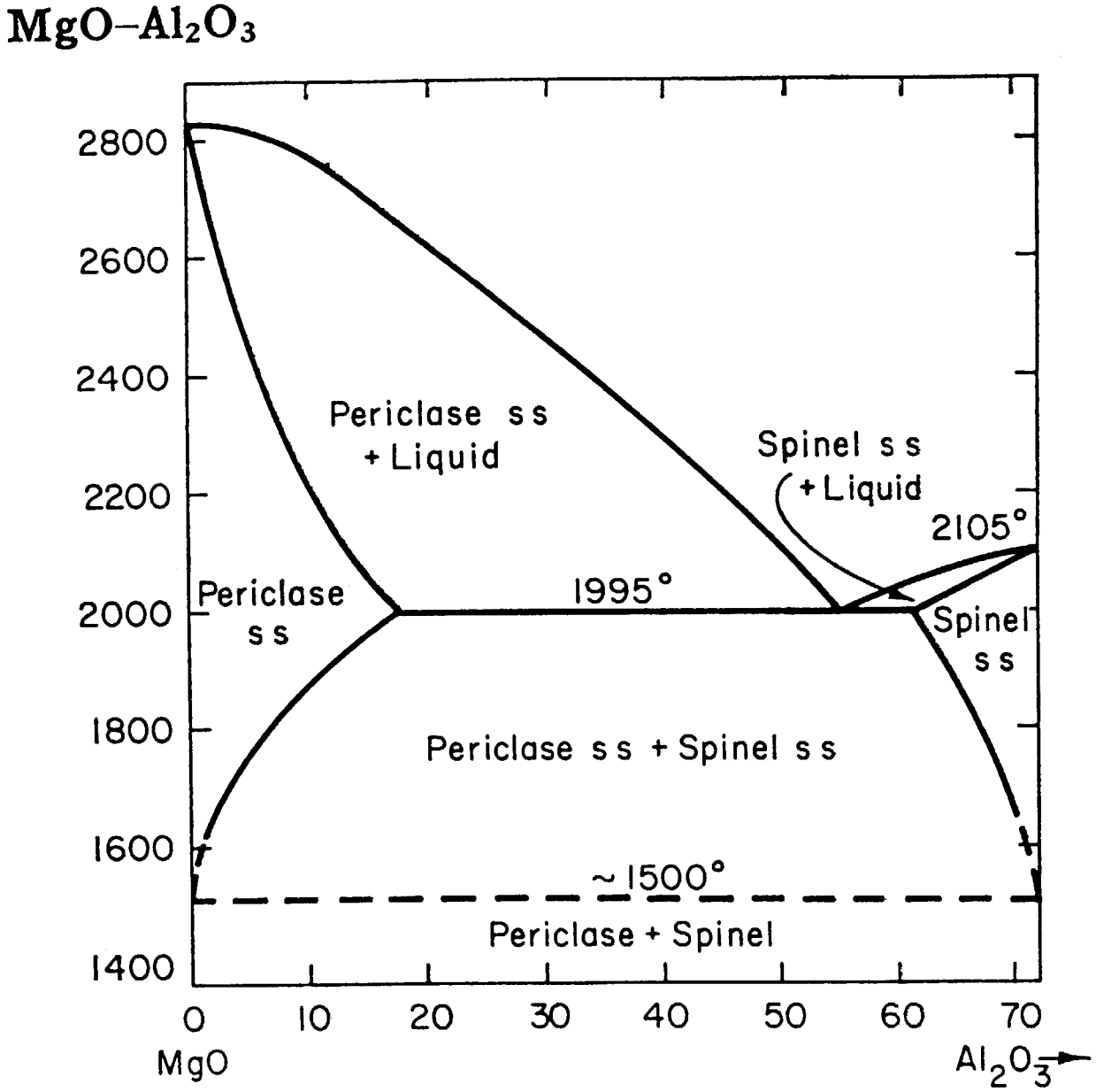

—System $MgO–MgO \cdot Al_2O_3$.

A. M. Alper, R. N. McNally, P. G. Ribbe, and R. C. Doman, *J. Am. Ceram. Soc.*, **45** [6] 264 (1962).

Fig. 7 Phase diagram of MgO-Al_2O_3 obtained from ref.(6).

Y_2O_3–ZrO_2

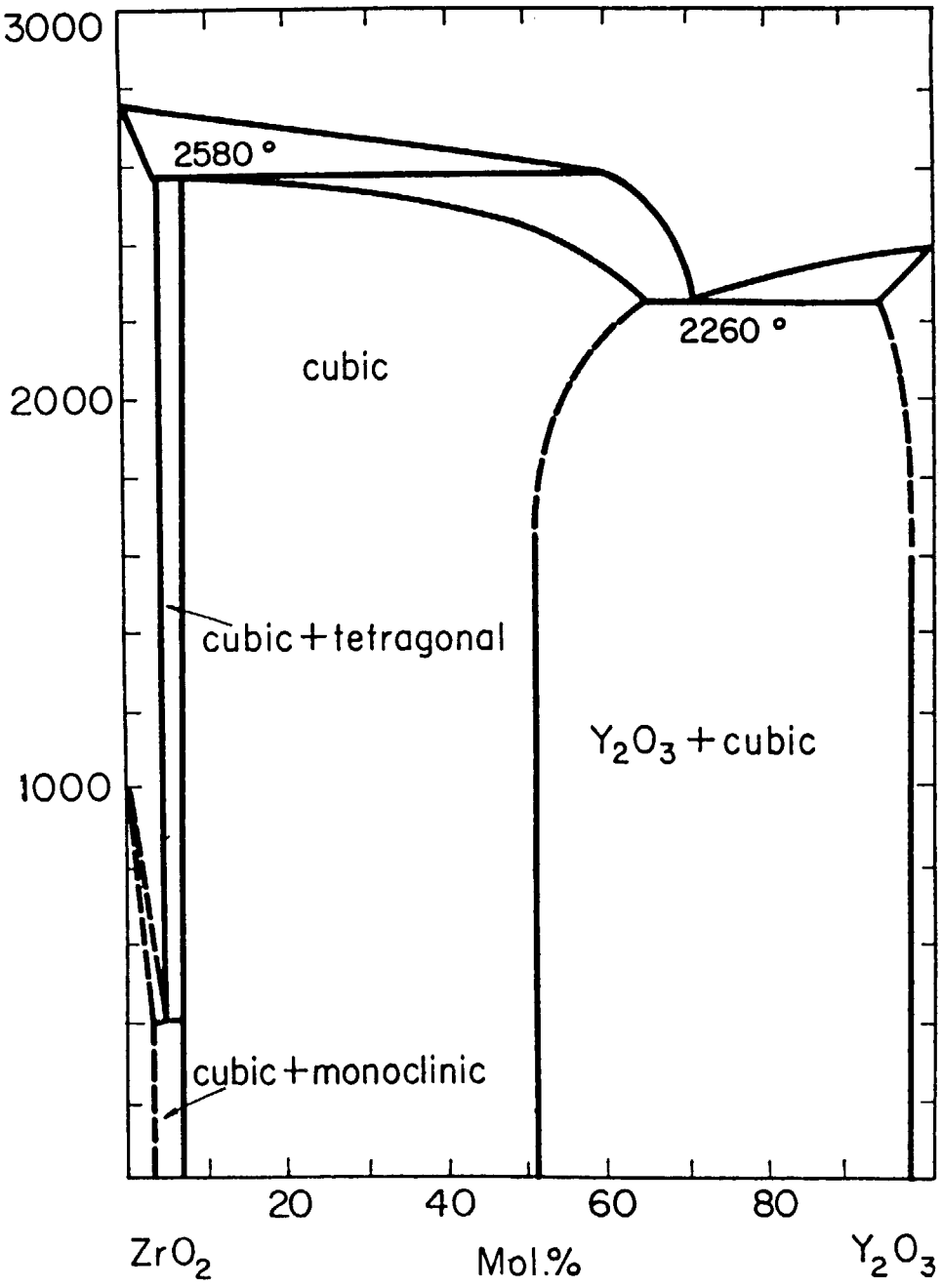

—System Y_2O_3–ZrO_2.

H. E. Otto, private communication Dec. 27, 1961. See also, P. S. Duwez, F. H. Brown, Jr., and F. Odell, *J. Electrochem. Soc.*, **98**, 360 (1951).

Fig. 8 Phase diagram of ZrO_2-Y_2O_3 obtained from ref.(6).

MgO–ZrO_2

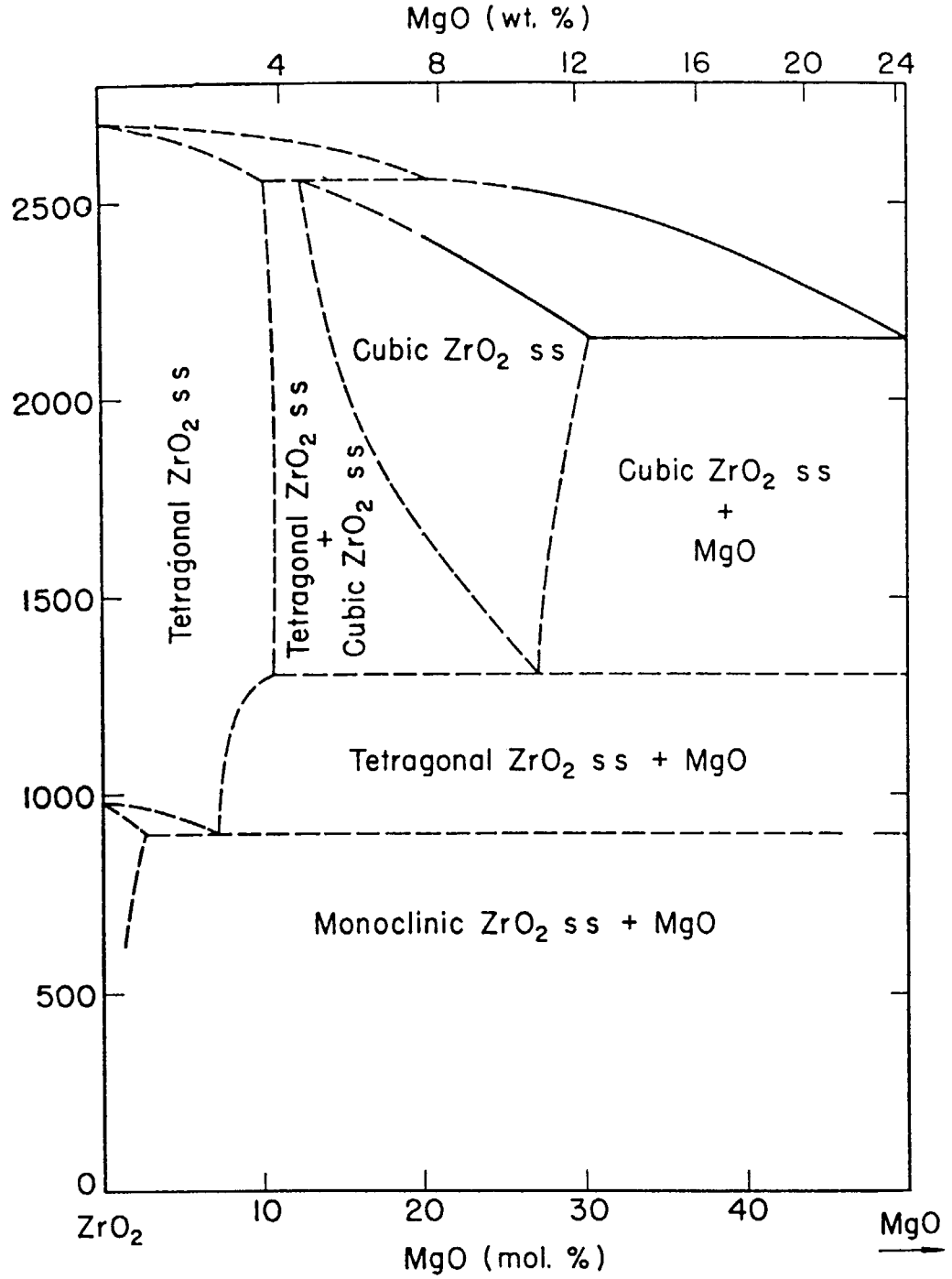

—System MgO–ZrO_2; tentative.

Pol Duwez, Francis Odell, and Frank H. Brown, Jr., *J. Am. Ceram. Soc.*, **35** [5] 109 (1952).

Fig. 9 Phase diagram of ZrO_2-MgO obtained from ref.(6).

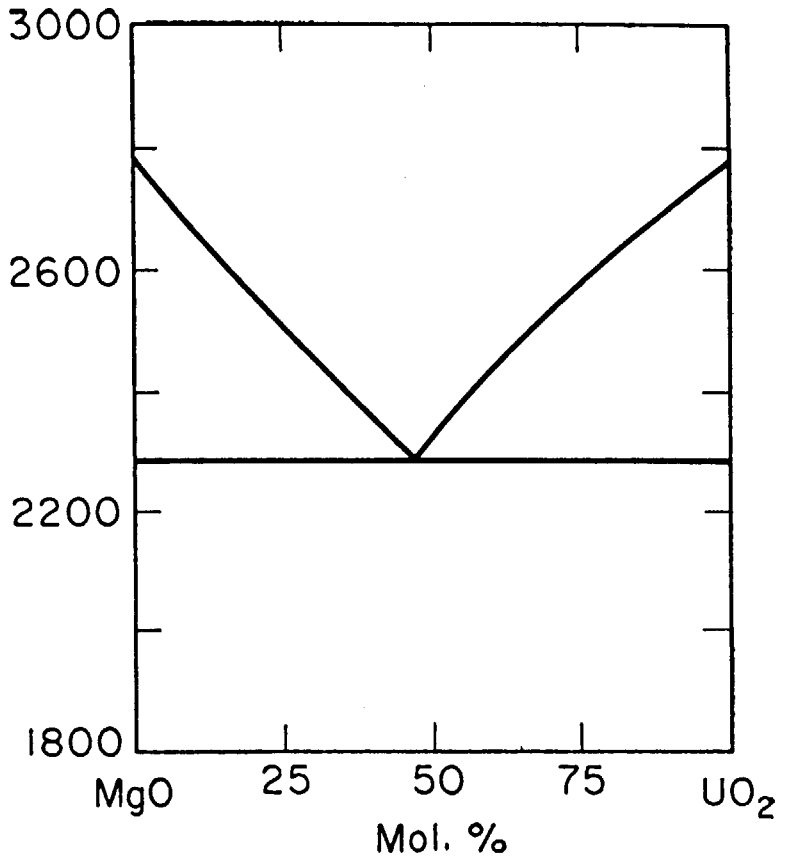

—System $MgO–UO_2$; idealized.

P. P. Budnikov, S. G. Tresvyatskiĭ, and V. I. Kushakovskiĭ, *Proc. U. N. Intern. Conf. Peaceful Uses At. Energy, 2nd, Geneva*, 6, 130 (1958).

Fig. 10 Phase diagram of MgO-UO_2 obtained from ref.(6).

Al_2O_3–UO_2

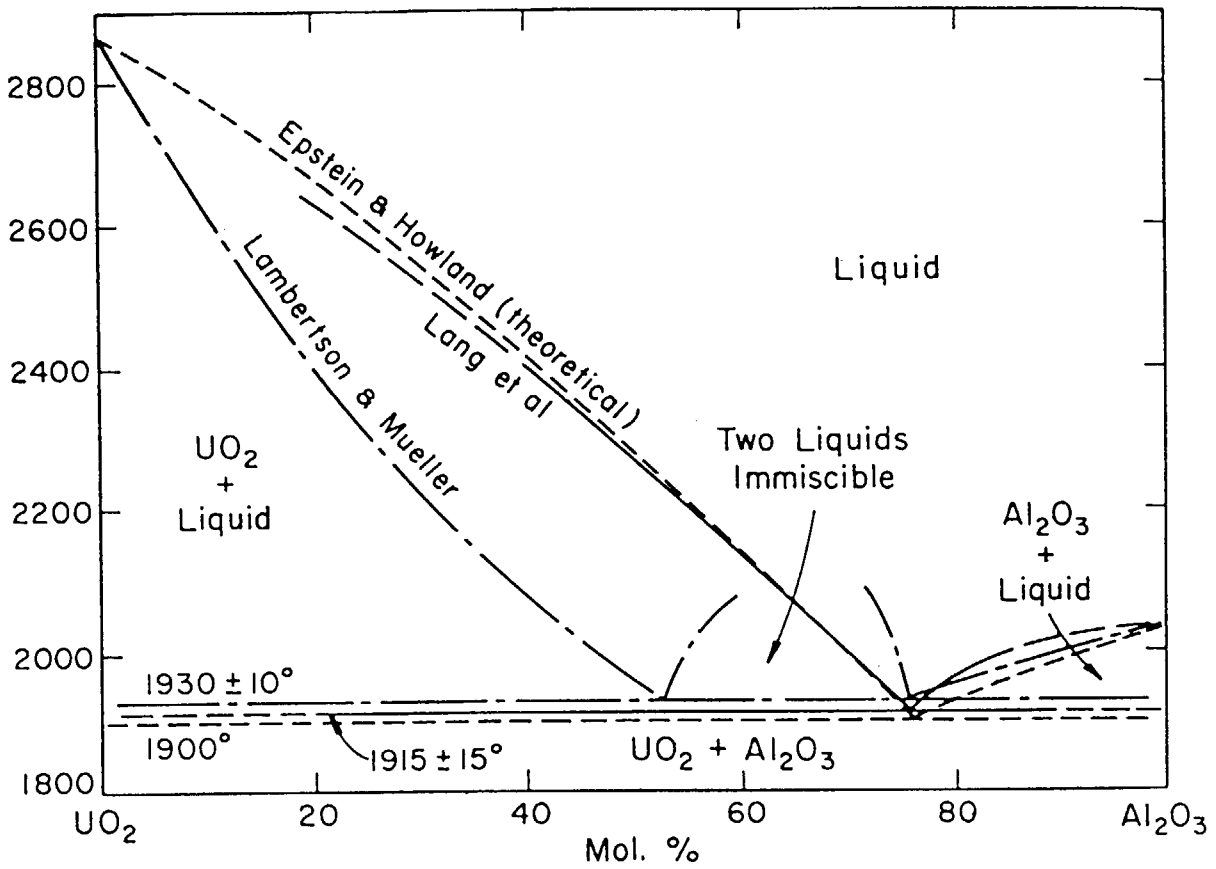

—System Al_2O_3–UO_2.

S. M. Lang, F. P. Knudsen, C. L. Fillmore, and R. S. Roth, *Natl. Bur. Standards Circ.*, No. 568, p. 14 (Feb. 20, 1956).

Fig. 11 Phase diagram of Al_2O_3 –UO_2 obtained from ref.(6).

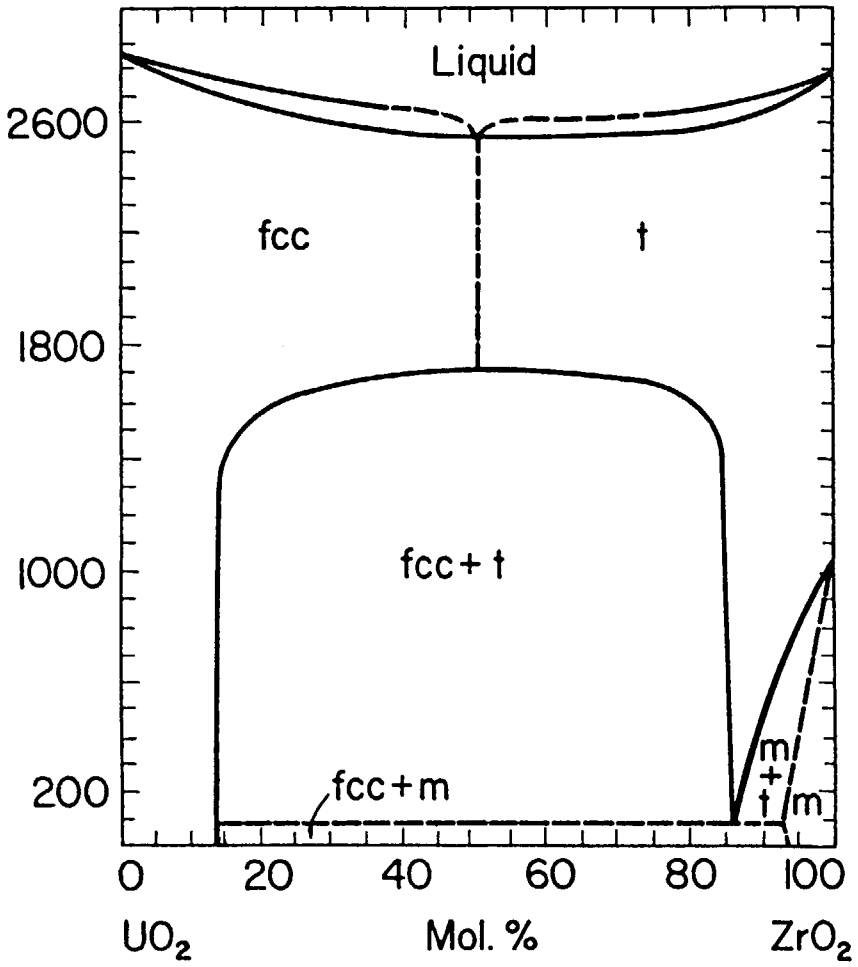

—System UO_2–ZrO_2. Solid solutions: fcc = face-centered cubic, m = monoclinic, t = tetragonal.

N. M. Voronov, E. A. Voitekhova, and A. S. Danilin, *Proc. U. N. Intern. Conf. Peaceful Uses At. Energy, 2nd, Geneva*, **6**, 223 (1958). Extent of immiscibility verified by E. Gebhardt and G. Elssner, Plansee Proc. 1961, pp. 133–39 (Publ. 1962) (in German).

For diagram showing smaller immiscibility gap in the subsolidus, see G. M. Wolten, *J. Am. Chem. Soc.*, **80**, 4774 (1958).

Fig. 12 Phase diagram of UO_2 –ZrO_2 obtained from ref.(6).

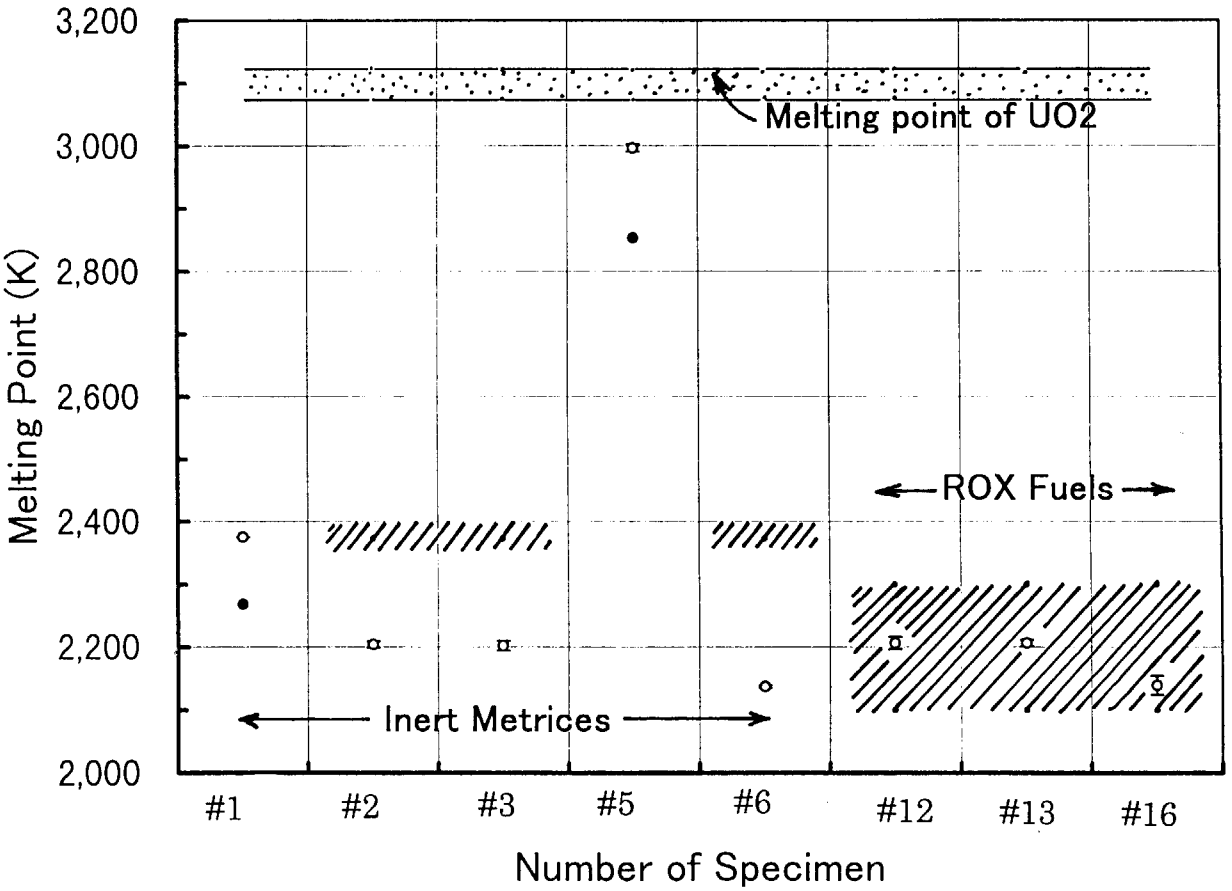

Fig. 13 MP of simulated ROX fuels and their inert matrices (open circles), where that of UO_2 (ref.(11)) is shown in dotted area. MP of simulated ROX fuels and their inert matrices estimated by the phase diagrams (ref.(6)) is shown in hatched area. Unit here is Kelvin (K) instead of Celsius(℃).

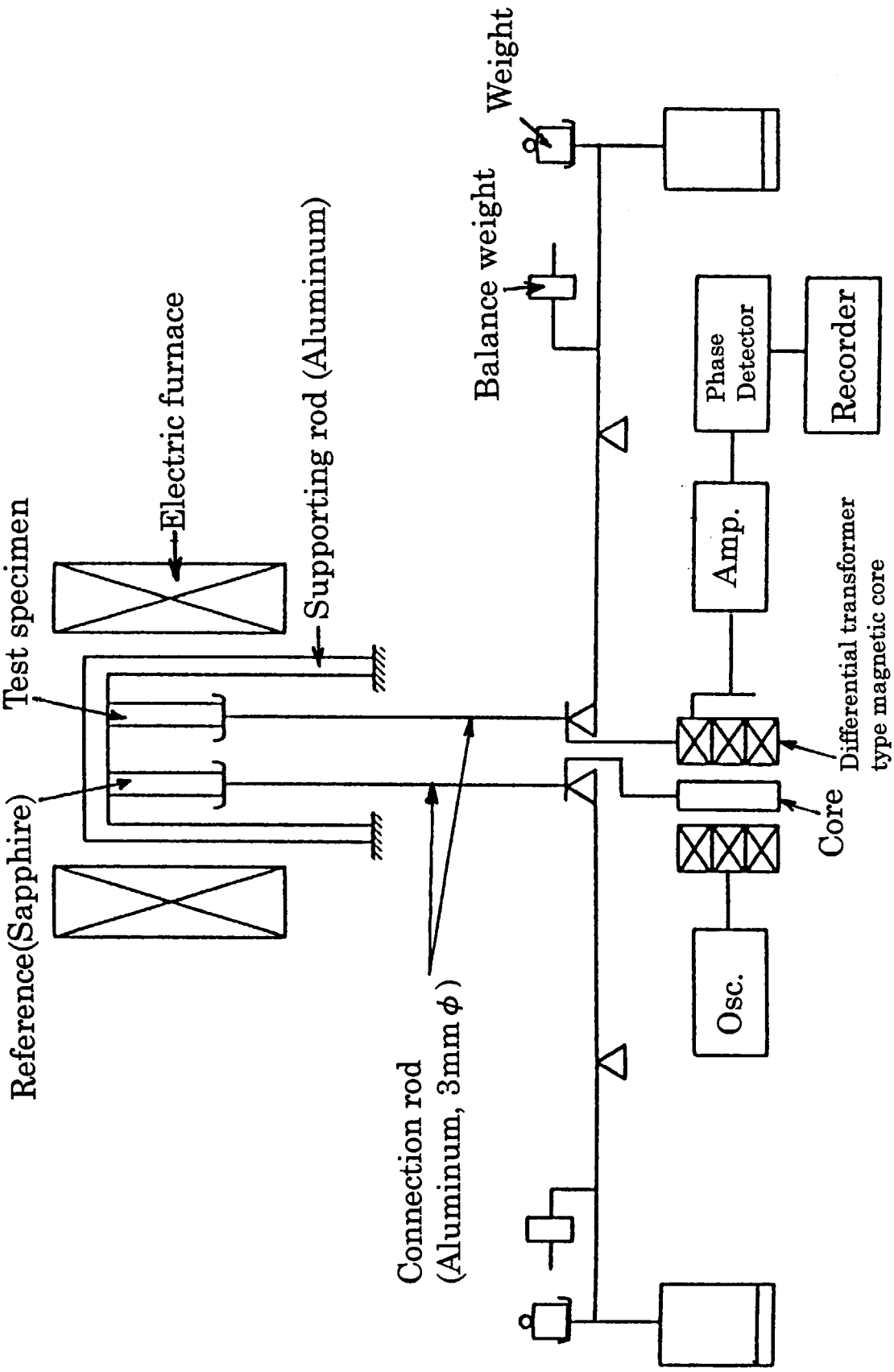

Fig. 14 Apparatus prepared for measuring LTE of simulated ROX fuels.

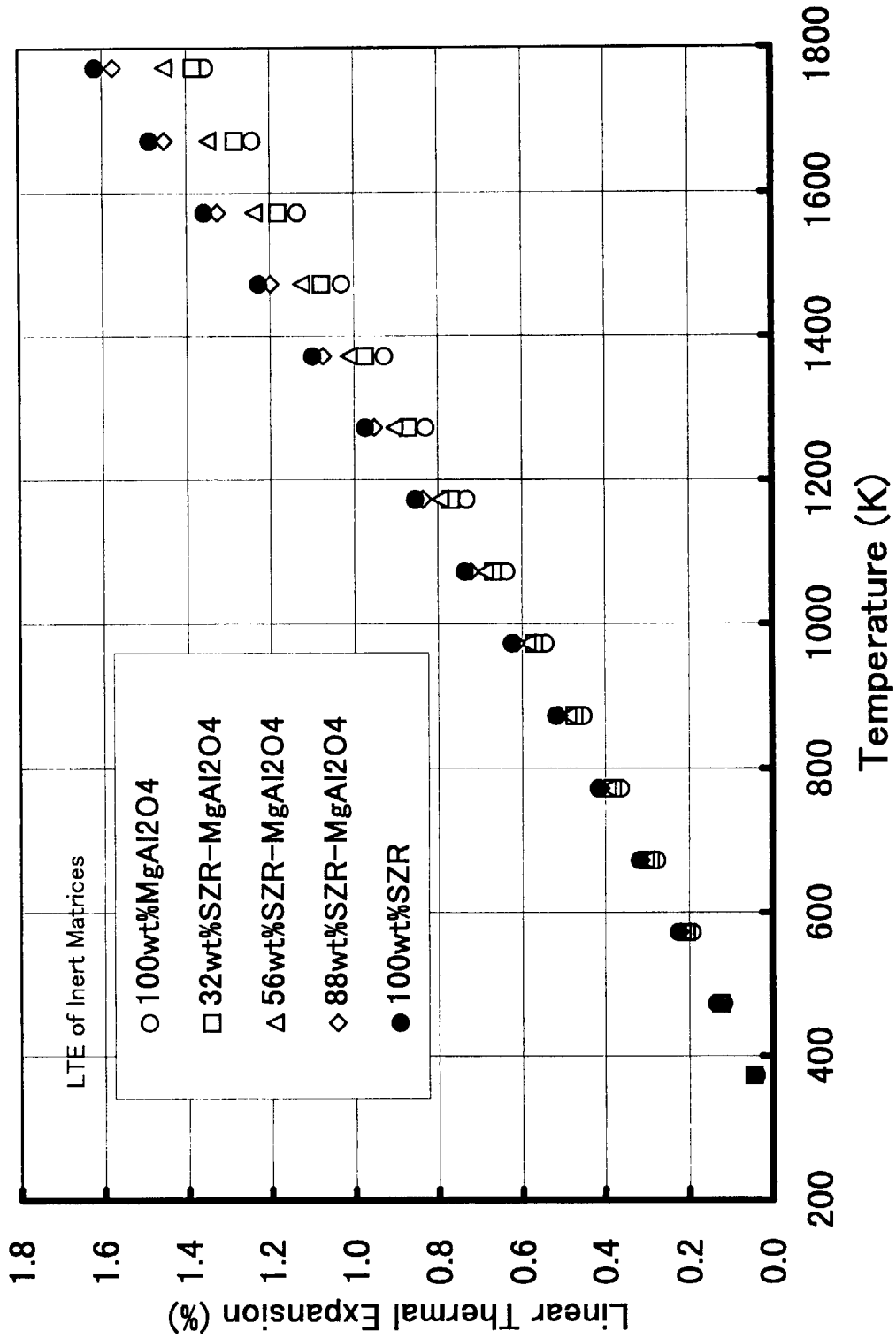

Fig. 15 LTE of inert matrices as a function of temperature

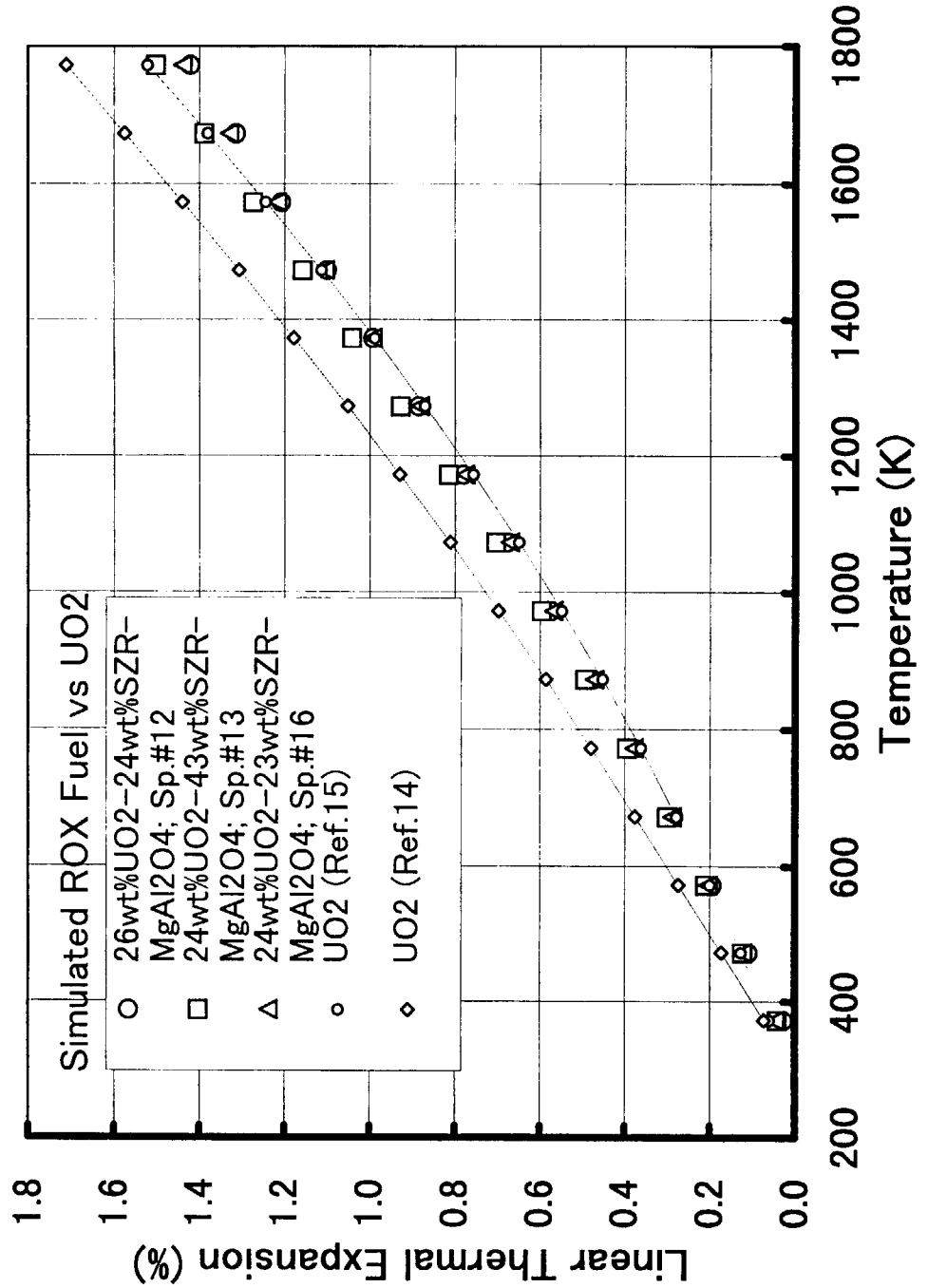

Fig. 16 LTE of simulated ROX fuels and UO_2 (ref.(14,15)) as a function of temperature

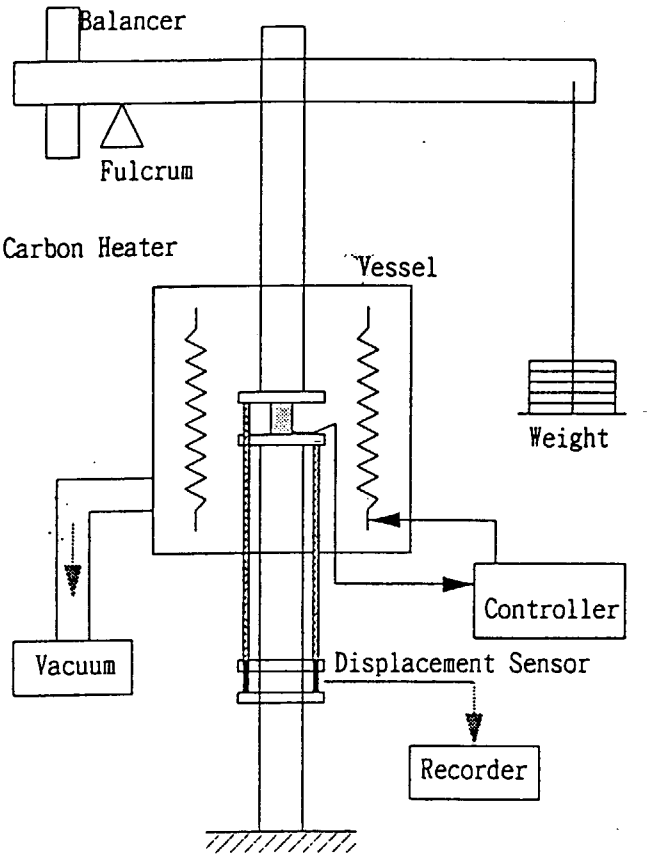

Fig. 17 Schematic diagram of apparatus used for measuring creep rate of simulated ROX fuel.

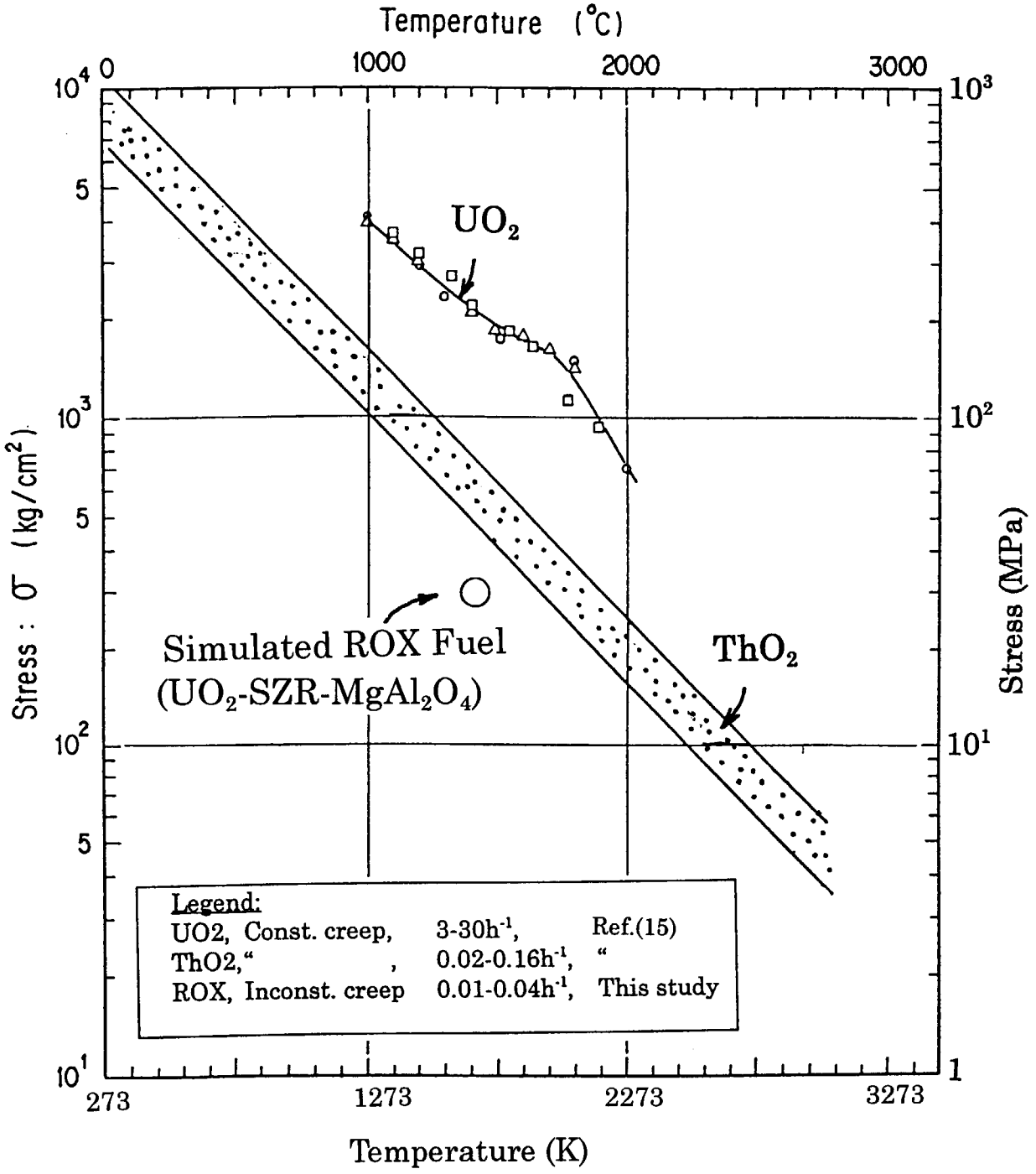

Fig. 18 Creep rate of simulated ROX fuel and that of UO_2 and ThO_2 (ref.(15)).

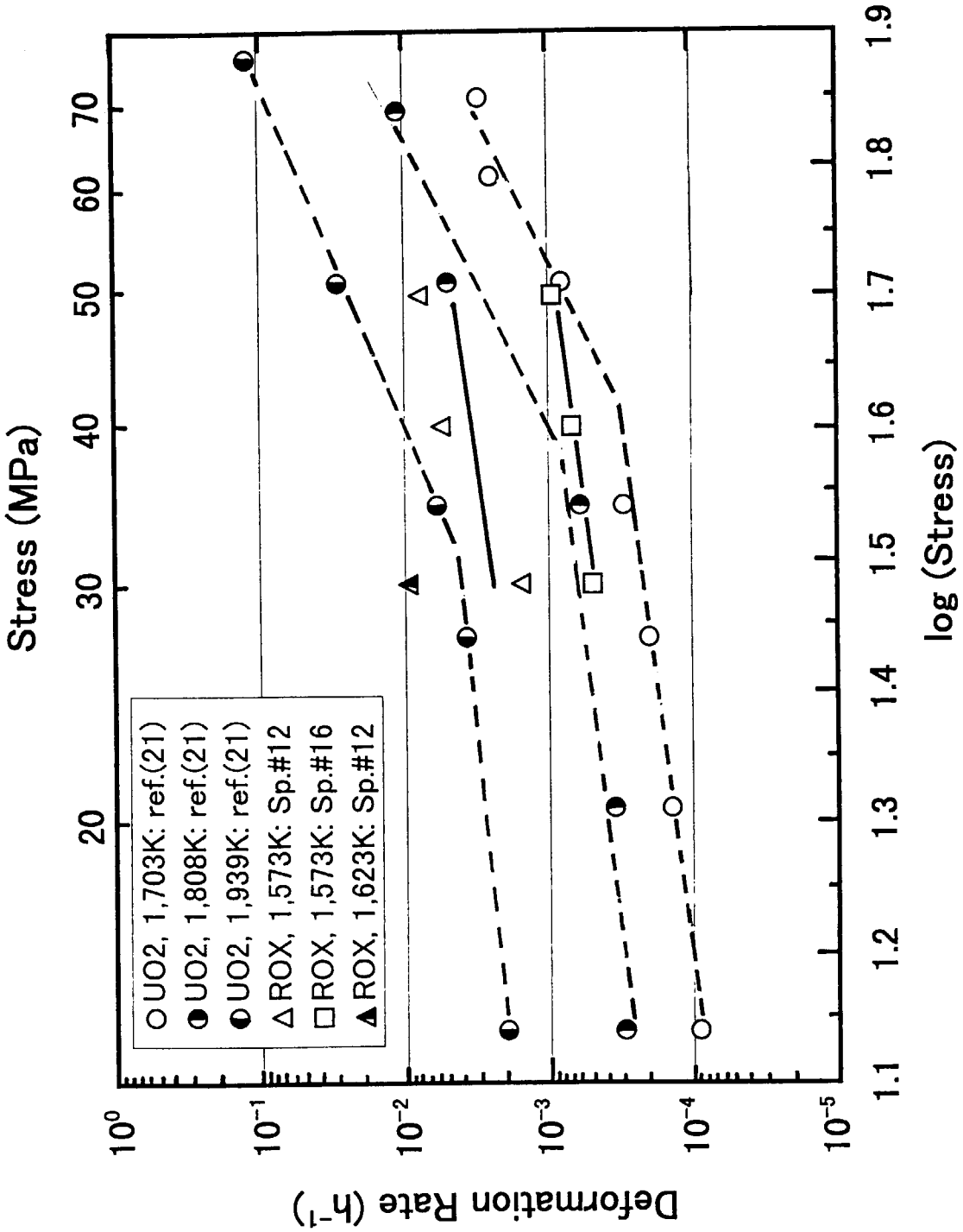

Fig. 19 Deformation rate of simulated ROX fuels and that of UO_2 (ref.(21)) at elevated temperatures.

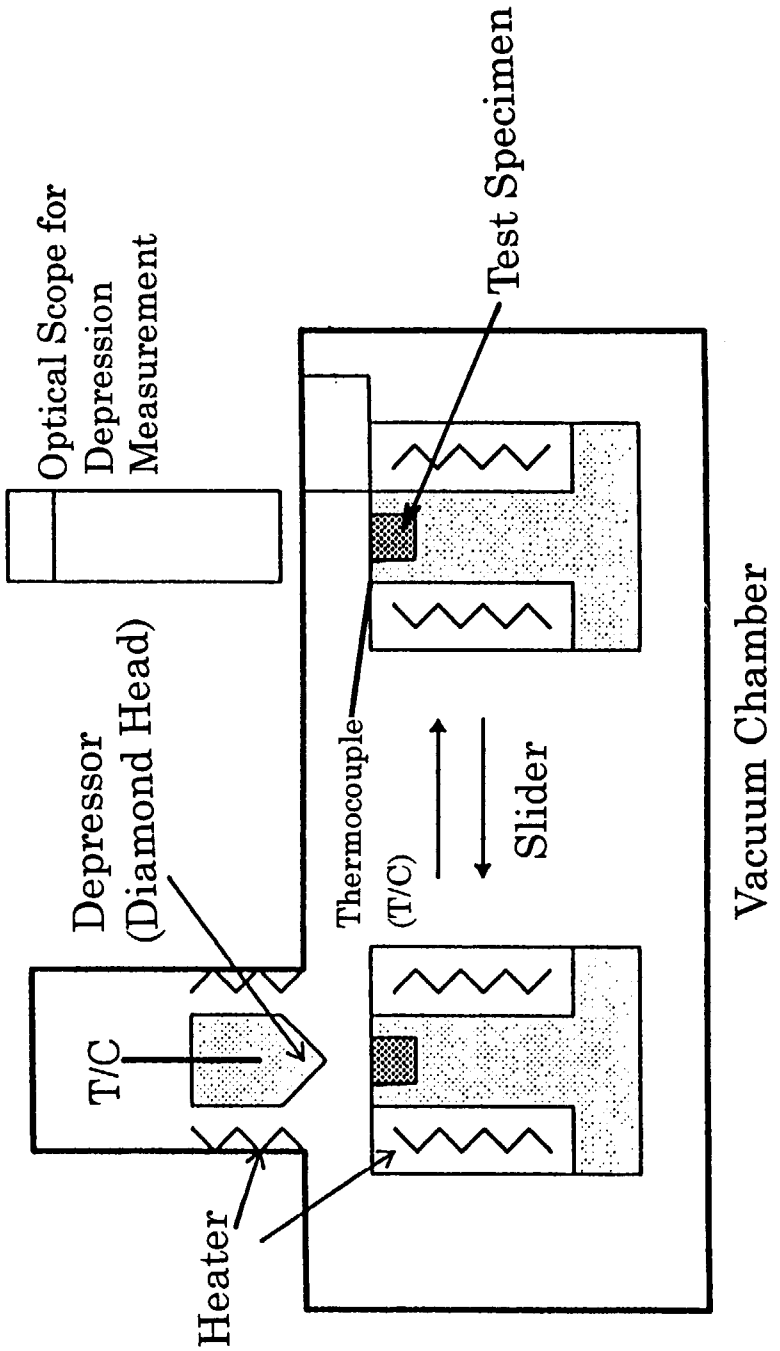

Fig. 20 Schematic representation showing an equipment for Hv measurement.

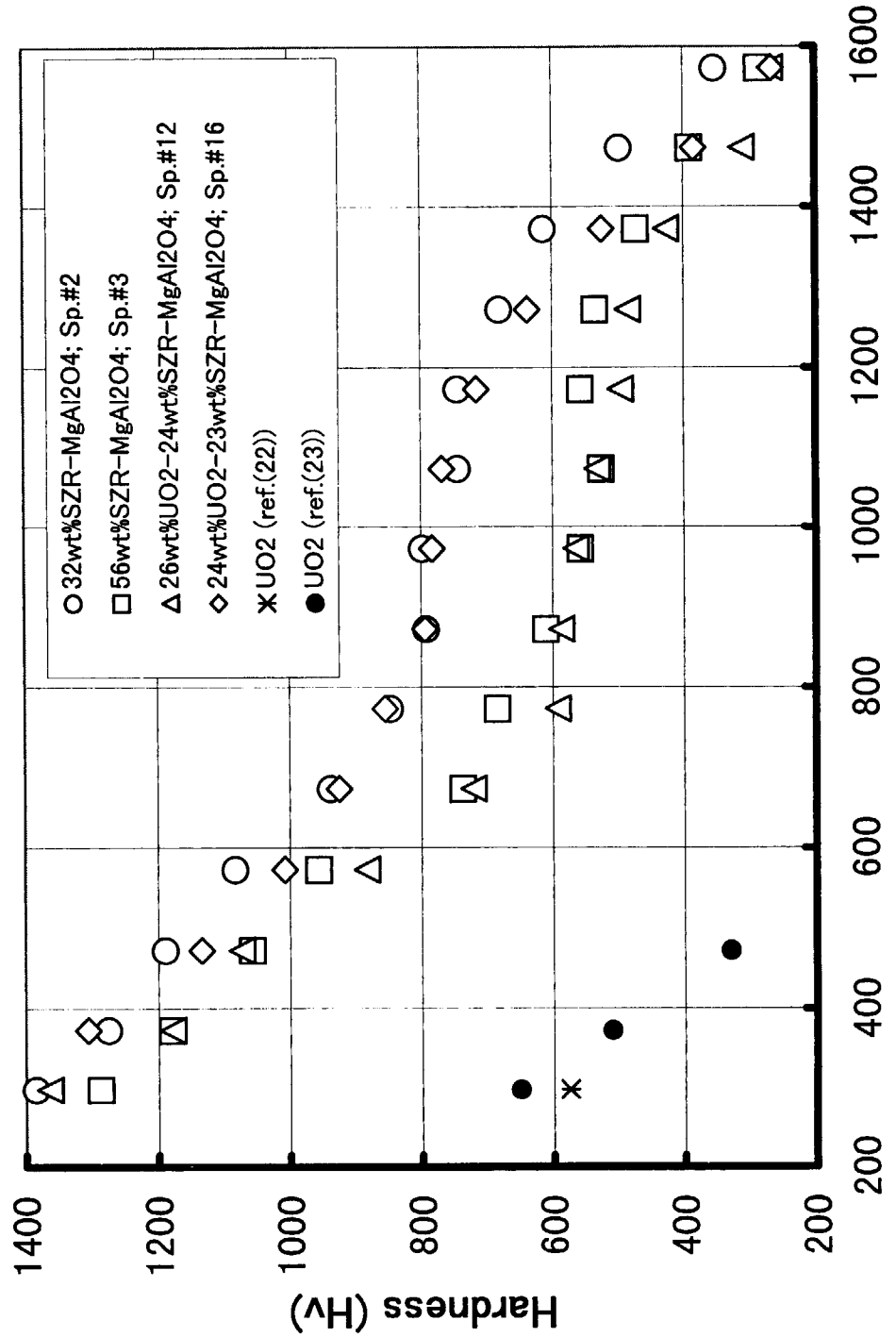

Fig. 21 Hv of two simulated ROX fuels (sp.#12, #16), two inert matrices (sp.#2, #3)) and UO_2 (ref.(22,23)) as a function of temperature.

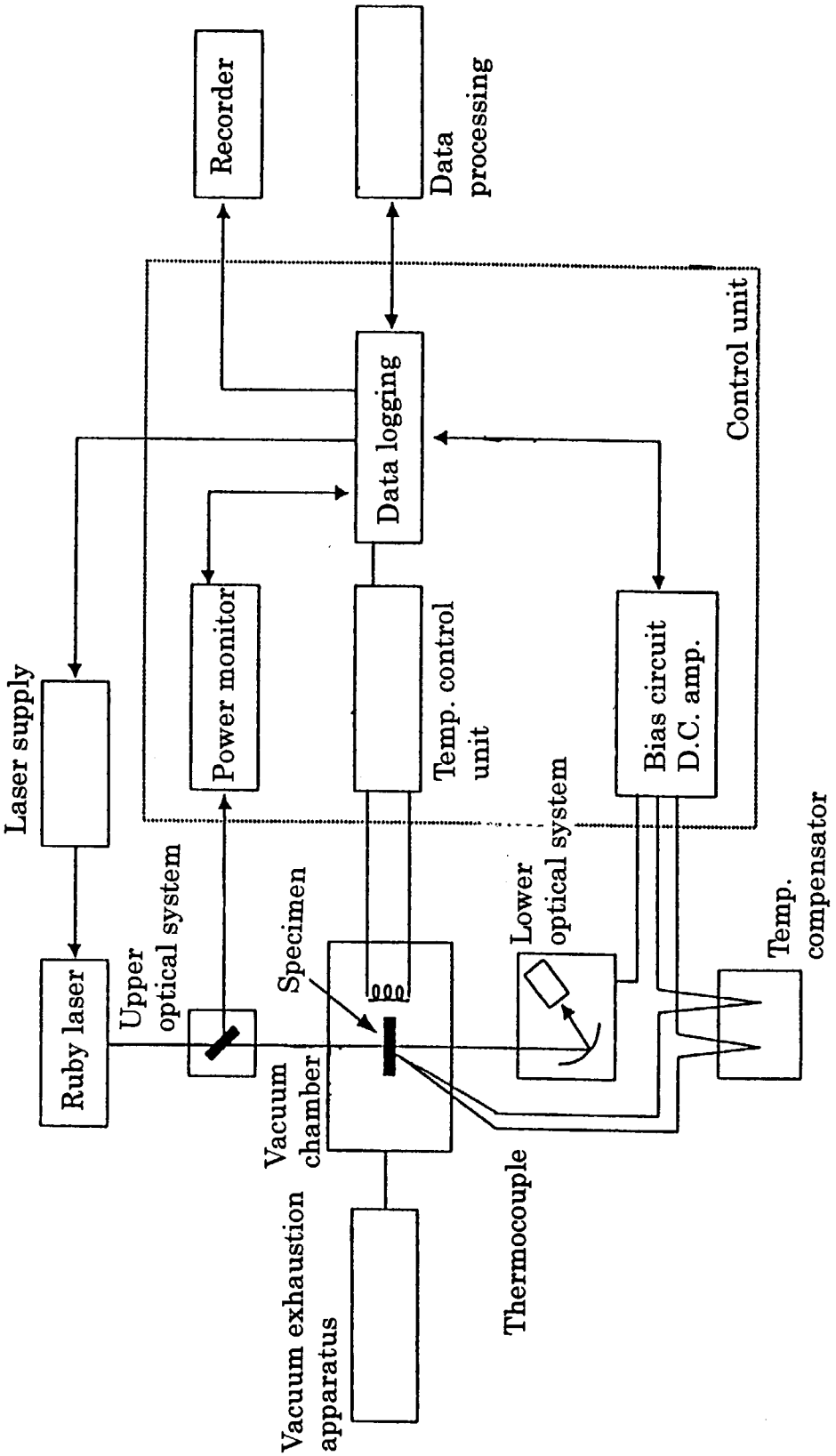

Fig. 22 Block diagram used for measuring the α_I .

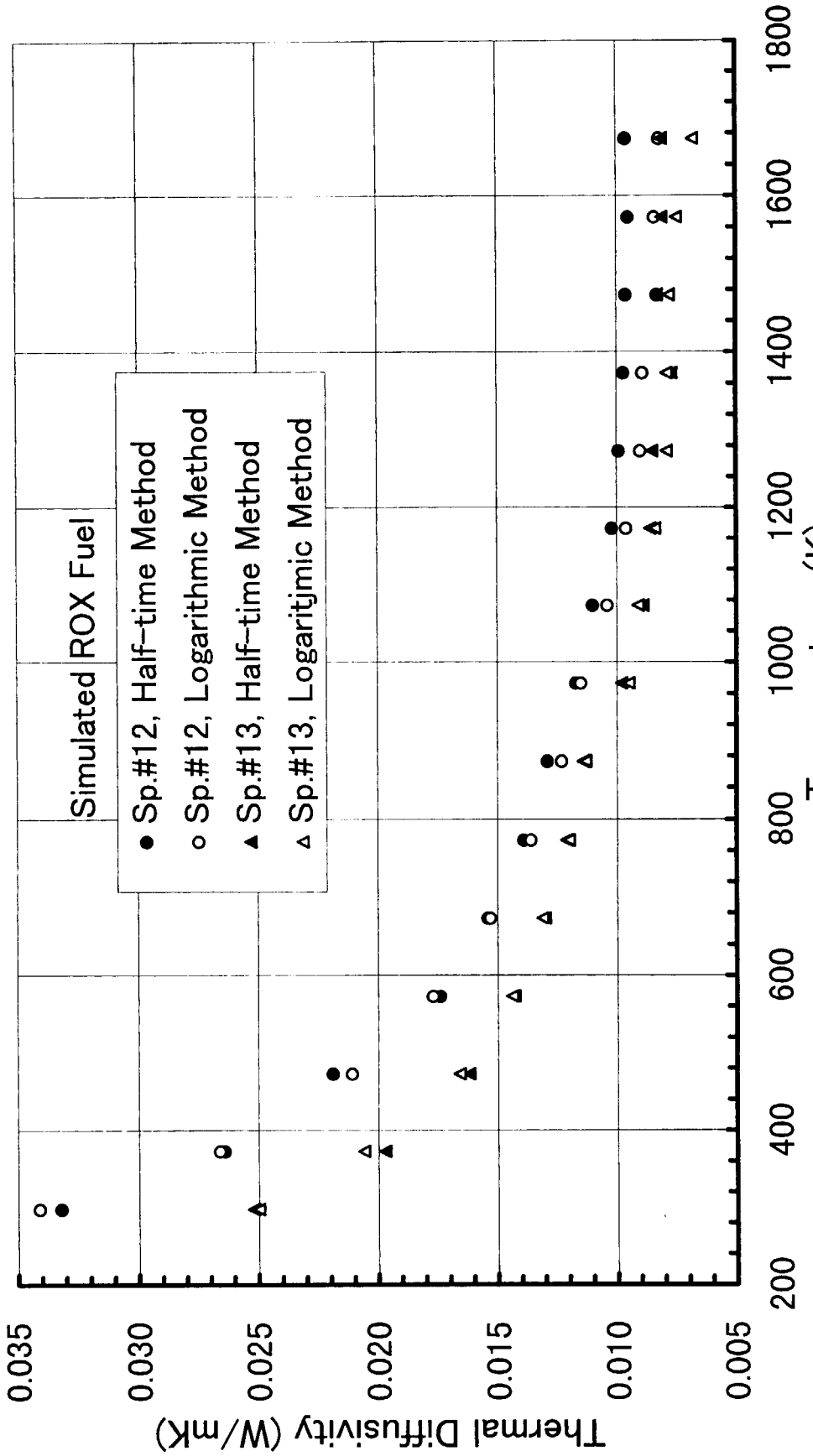

Fig. 23 Comparison between thermal diffusivity measured by half-time method and that measured by logarithmic method

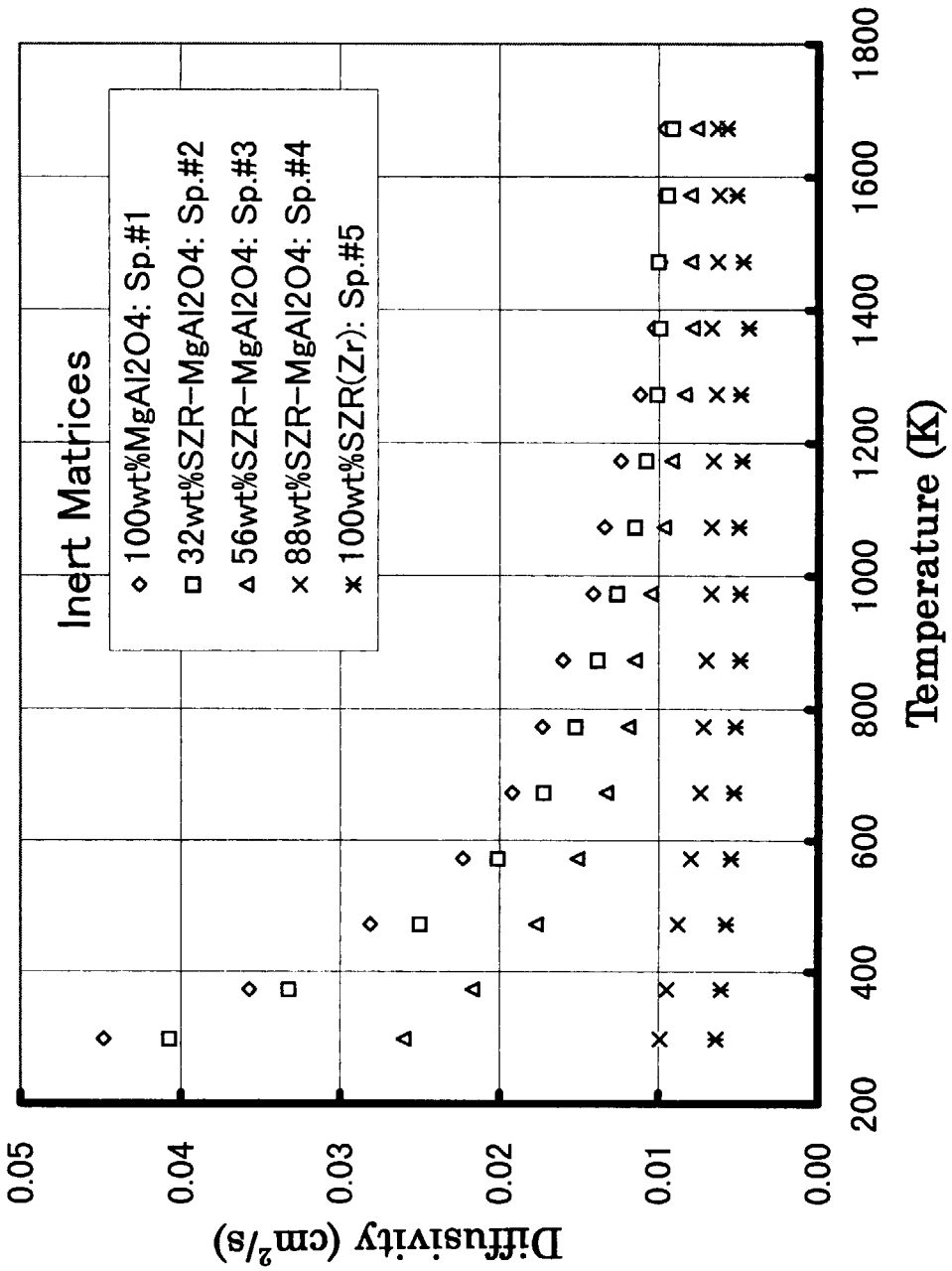

Fig. 24 The α, of test specimens #1(◇), #2(□), #3(△), #4(X), and #5(*) as a function of temperature.

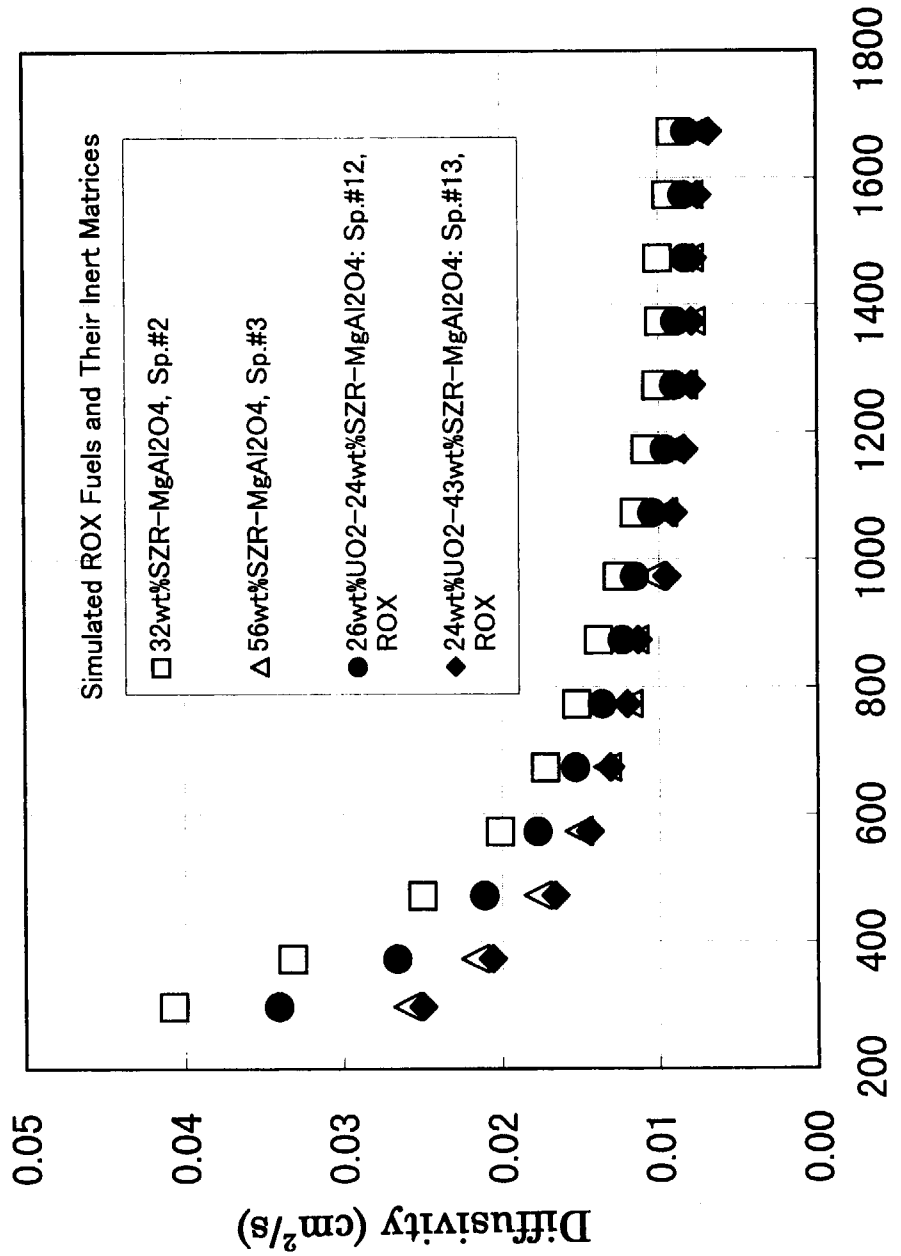

Fig. 25 The α_f of simulated ROX fuels (full marks) and references (open marks) as a function of temperature.

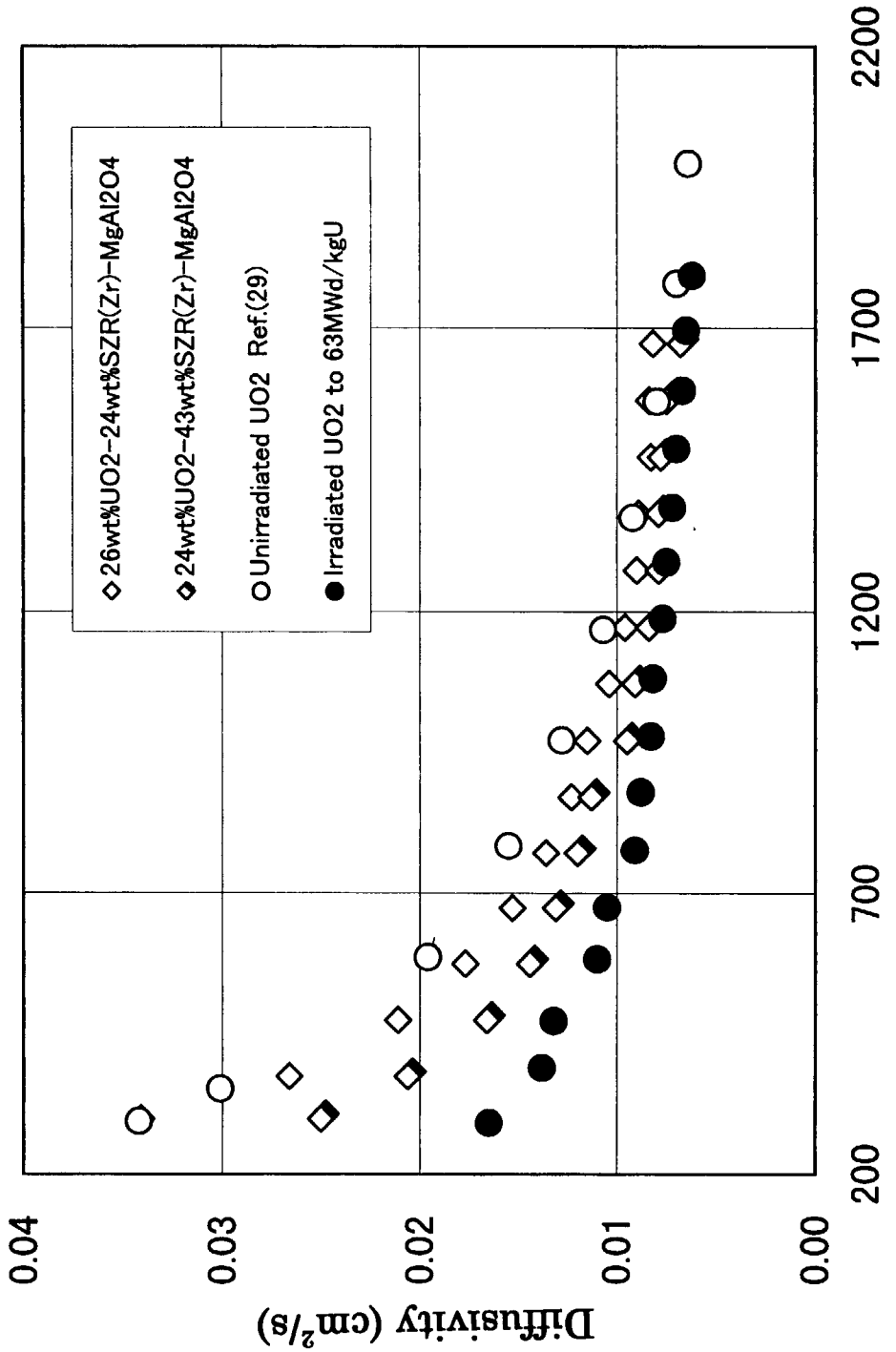

Fig. 26 The α_f of simulated ROX fuels (diamonds) and UO_2 (circles, ref.(29)) as a function of temperature.

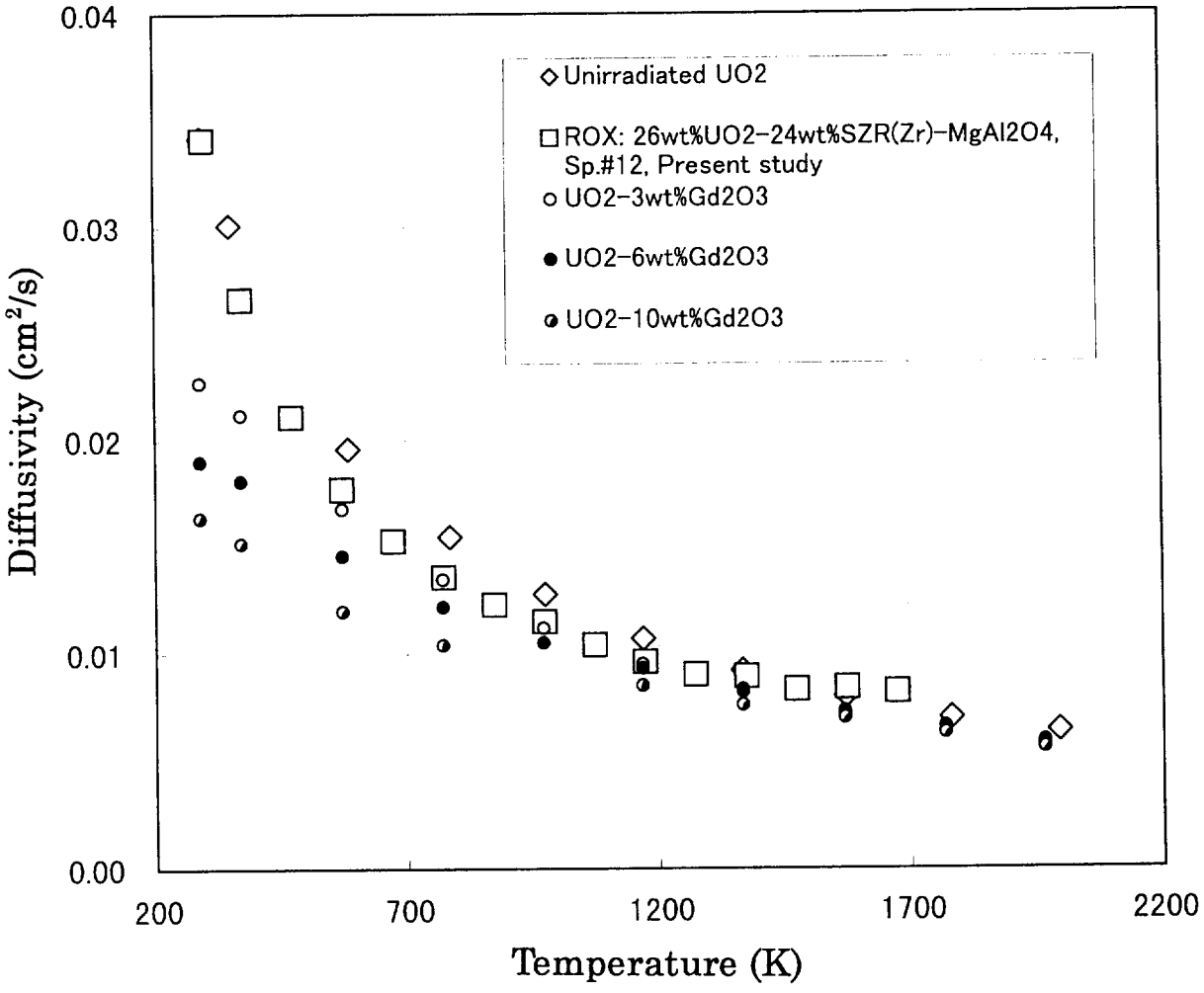

Fig. 27 The α_l of UO_2 (◇, ref.(29)), simulated ROX fuel(□) and Gd_2O_3 doped UO_2 (circles, ref.(30)) as a function of temperature.

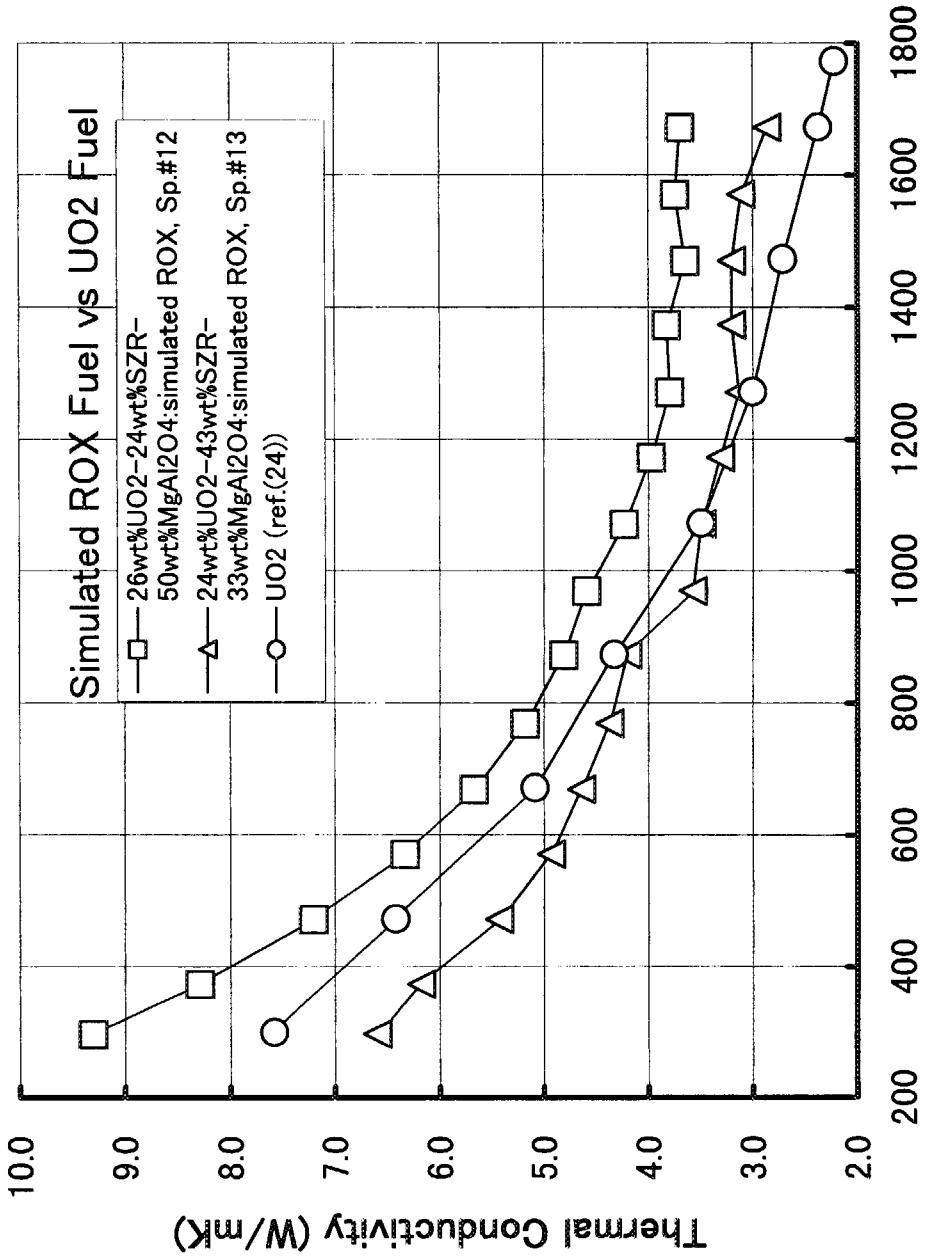

Fig. 28 Thermal conductivity of simulated ROX fuels and UO_2 (ref.(24)) as a function of temperature.

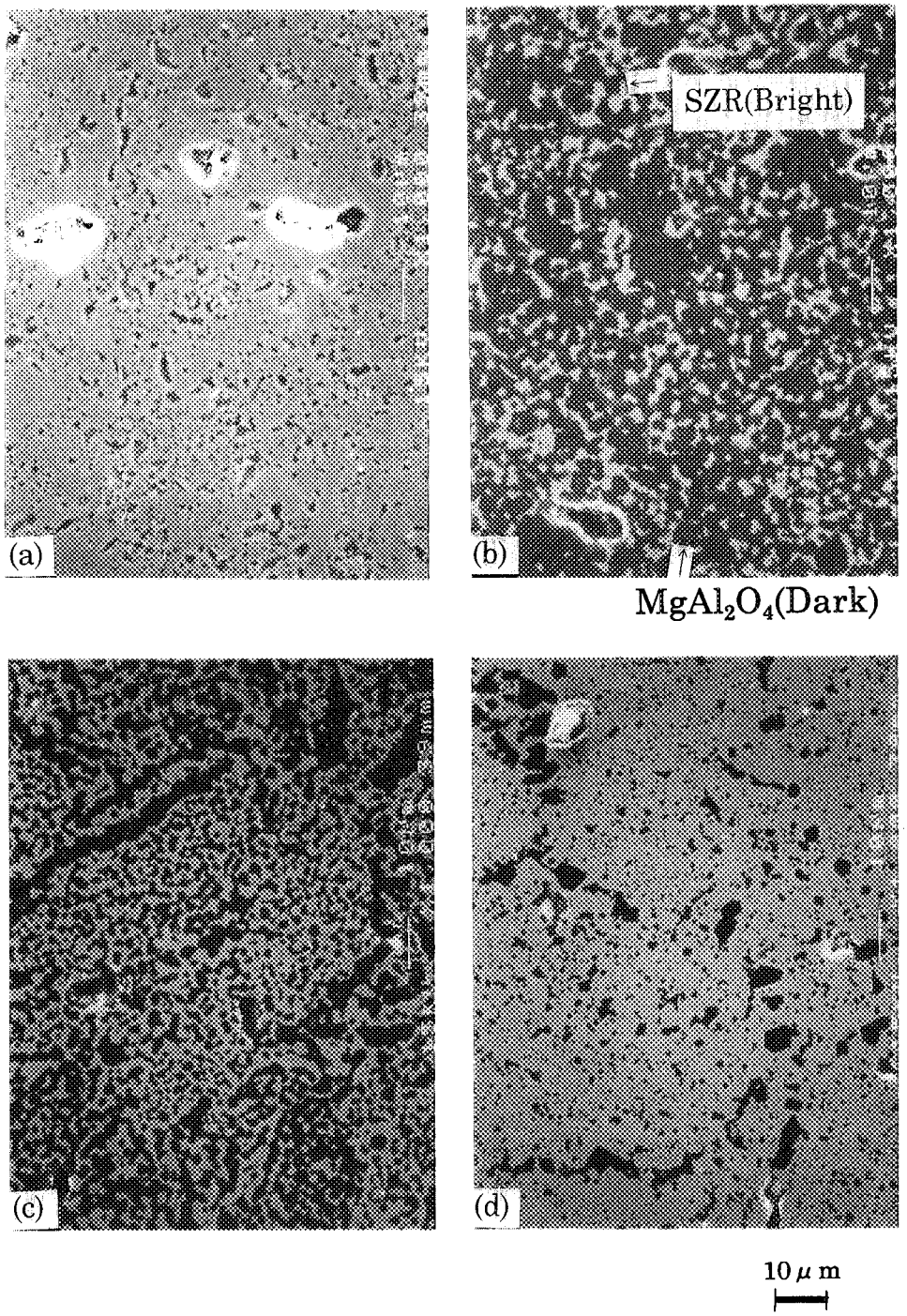

Photo. 1 As-fabricated microstructure (SEM image) of simulated ROX fuel:
(a) Specimen#1, $MgAl_2O_4$ single phase,
(b) Sp.#2, 32wt%SZR-$MgAl_2O_4$, (c) Sp.#3, 56wt%SZR-$MgAl_2O_4$,
(d) Sp.#4, 88wt%SZR-$MgAl_2O_4$

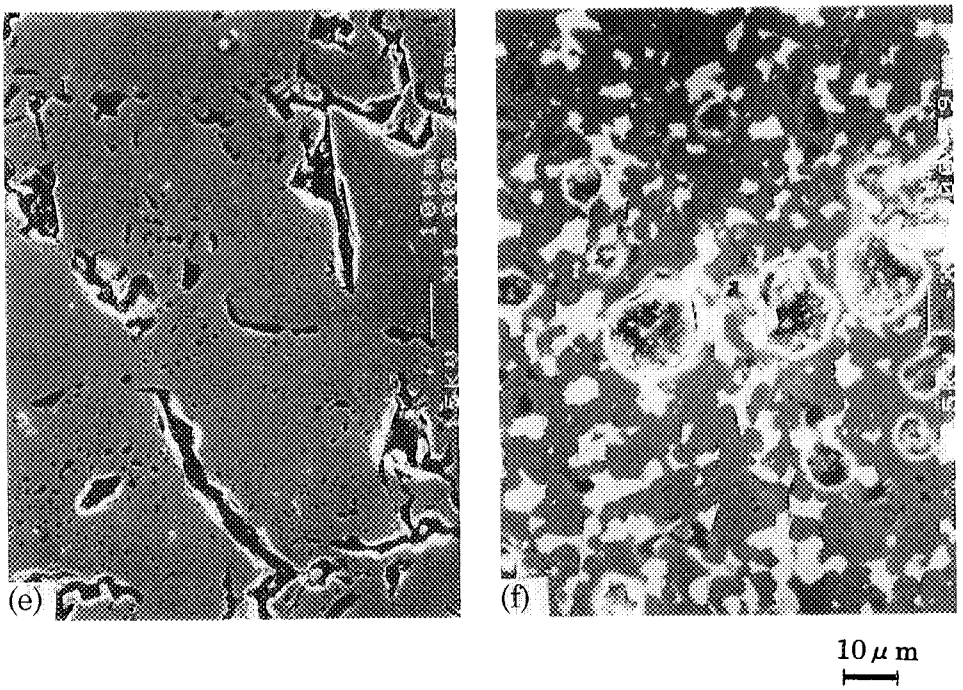

Photo. 1 (Continued)
As-fabricated microstructure (SEM image) of simulated ROX fuel:
(e) Sp.#5, SZR single phase,
(f) Sp.#6, 30wt%SZR-$MgAl_2O_4$

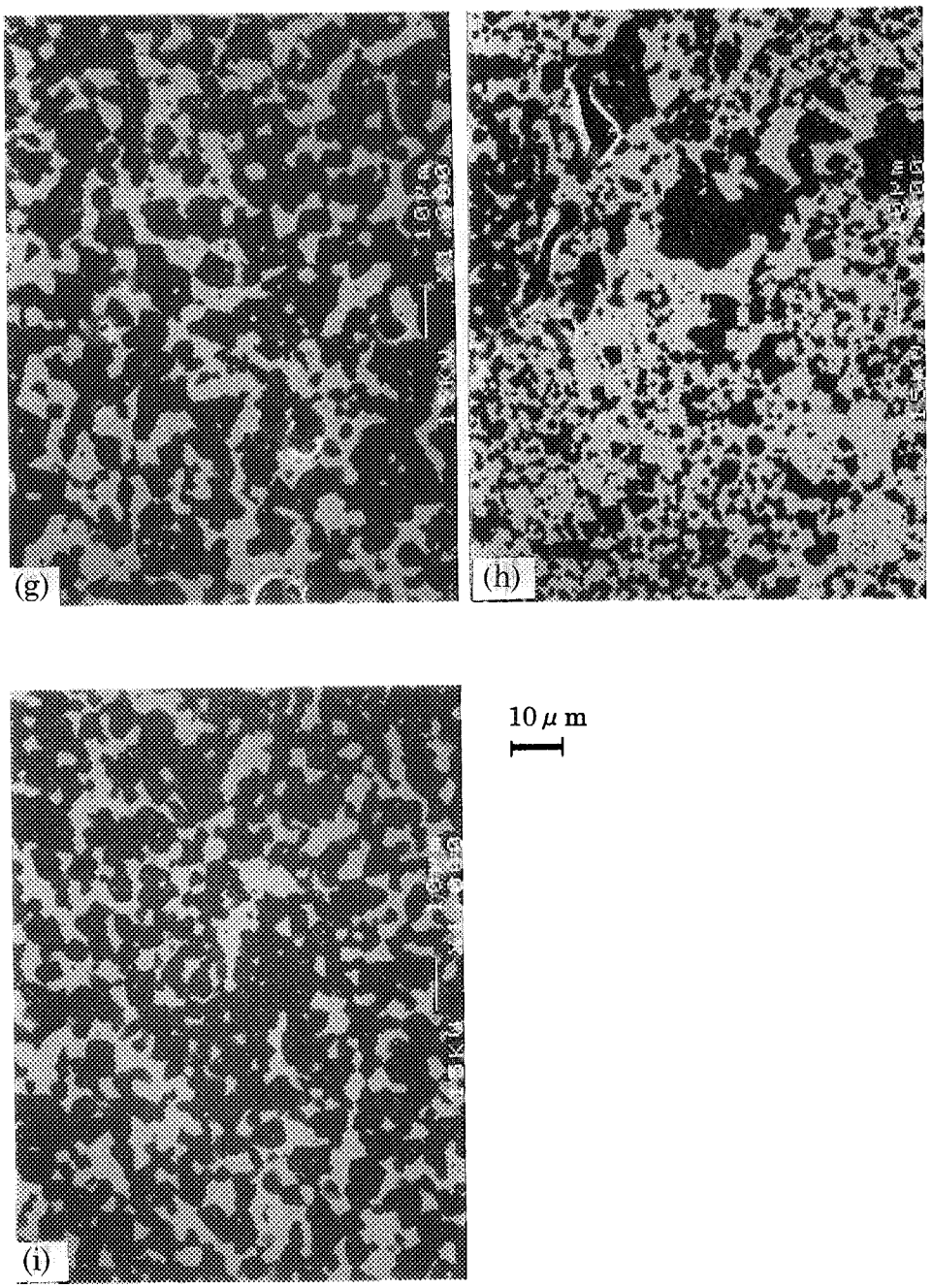

Photo. 1 (Continued)
As-fabricated microstructure (SEM image) of simulated ROX fuel:
(g) Sp.#12, 26wt%UO_2-24wt%SZR-$MgAl_2O_4$,
(h) Sp.#13, 24wt%UO_2-43wt%SZR-$MgAl_2O_4$,
(i) Sp.#16, 24wt%UO_2-23wt%SZR-$MgAl_2O_4$

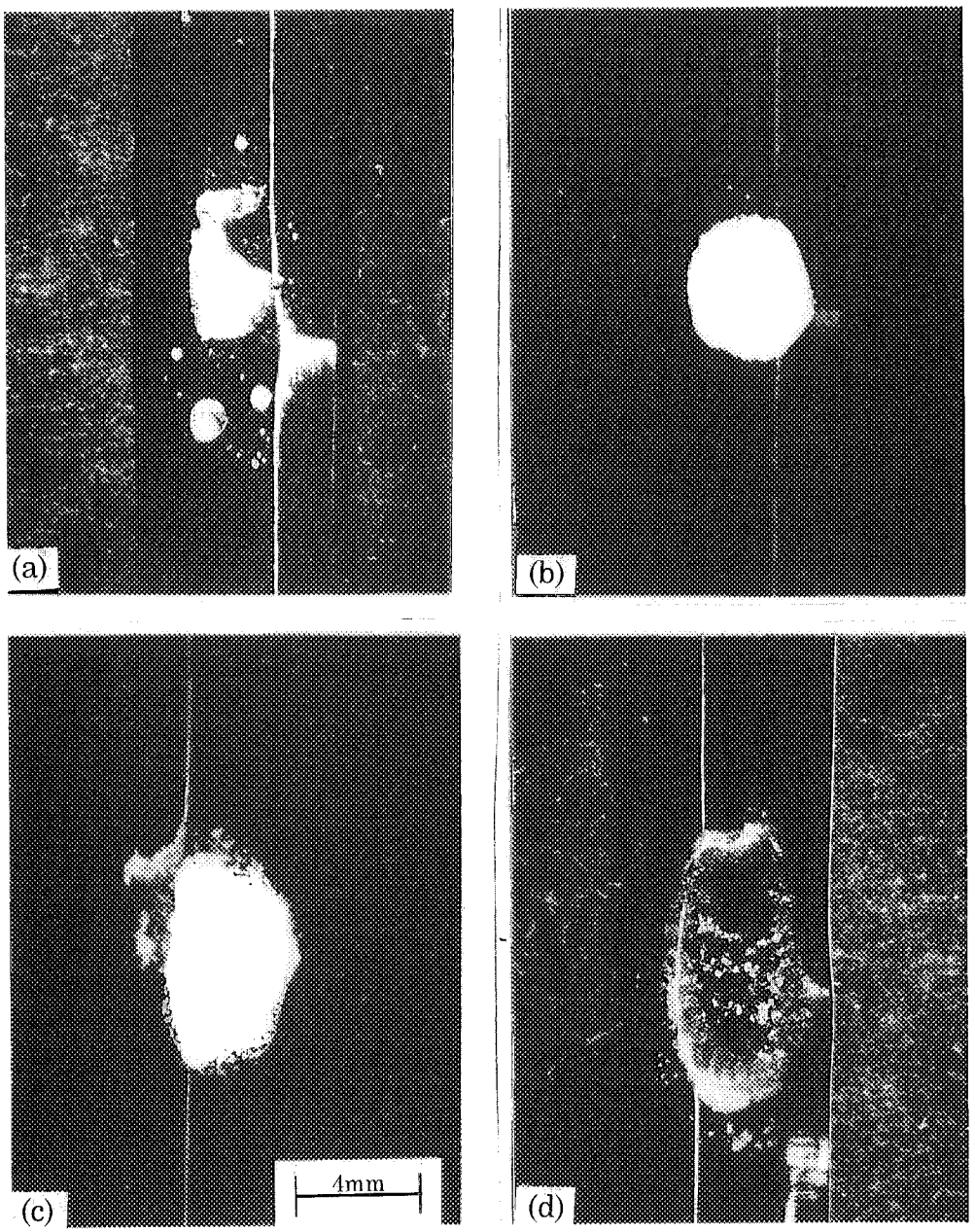

Photo. 2 Morphology of three test specimens provided for MP test done by thermal arrest method:
(a) Sp.#1, $MgAl_2O_4$ single phase,
(b) Sp.#2, 32wt%SZR-$MgAl_2O_4$,
(c) Sp.#3, 56wt%SZR-$MgAl_2O_4$,
(d) Sp.#5, SZR single phase.

This is a blank page.

国際単位系 (SI) と換算表

表1　SI基本単位および補助単位

量	名称	記号
長さ	メートル	m
質量	キログラム	kg
時間	秒	s
電流	アンペア	A
熱力学温度	ケルビン	K
物質量	モル	mol
光度	カンデラ	cd
平面角	ラジアン	rad
立体角	ステラジアン	sr

表2　SIと併用される単位

名称	記号
分，時，日	min，h，d
度，分，秒	°，′，″
リットル	l，L
トン	t
電子ボルト	eV
原子質量単位	u

1 eV = 1.60218 × 10^{-19} J

1 u = 1.66054 × 10^{-27} kg

表5　SI接頭語

倍数	接頭語	記号
10^{18}	エクサ	E
10^{15}	ペタ	P
10^{12}	テラ	T
10^{9}	ギガ	G
10^{6}	メガ	M
10^{3}	キロ	k
10^{2}	ヘクト	h
10^{1}	デカ	da
10^{-1}	デシ	d
10^{-2}	センチ	c
10^{-3}	ミリ	m
10^{-6}	マイクロ	μ
10^{-9}	ナノ	n
10^{-12}	ピコ	p
10^{-15}	フェムト	f
10^{-18}	アト	a

表3　固有の名称をもつSI組立単位

量	名称	記号	他のSI単位による表現
周波数	ヘルツ	Hz	s^{-1}
力	ニュートン	N	$m \cdot kg/s^2$
圧力，応力	パスカル	Pa	N/m^2
エネルギー，仕事，熱量	ジュール	J	N·m
工率，放射束	ワット	W	J/s
電気量，電荷	クーロン	C	A·s
電位，電圧，起電力	ボルト	V	W/A
静電容量	ファラド	F	C/V
電気抵抗	オーム	Ω	V/A
コンダクタンス	ジーメンス	S	A/V
磁束	ウェーバ	Wb	V·s
磁束密度	テスラ	T	Wb/m^2
インダクタンス	ヘンリー	H	Wb/A
セルシウス温度	セルシウス度	℃	
光束	ルーメン	lm	cd·sr
照度	ルクス	lx	lm/m^2
放射能	ベクレル	Bq	s^{-1}
吸収線量	グレイ	Gy	J/kg
線量当量	シーベルト	Sv	J/kg

表4　SIと共に暫定的に維持される単位

名称	記号
オングストローム	Å
バーン	b
バール	bar
ガル	Gal
キュリー	Ci
レントゲン	R
ラド	rad
レム	rem

1 Å = 0.1 nm = 10^{-10} m

1 b = 100 fm^2 = 10^{-28} m^2

1 bar = 0.1 MPa = 10^5 Pa

1 Gal = 1 cm/s^2 = 10^{-2} m/s^2

1 Ci = 3.7 × 10^{10} Bq

1 R = 2.58 × 10^{-4} C/kg

1 rad = 1 cGy = 10^{-2} Gy

1 rem = 1 cSv = 10^{-2} Sv

（注）

1. 表1－5は「国際単位系」第5版，国際度量衡局 1985年刊行による。ただし，1 eVおよび1 uの値はCODATAの1986年推奨値によった。
2. 表4には海里，ノット，アール，ヘクタールも含まれているが日常の単位なのでここでは省略した。
3. barは，JISでは流体の圧力を表わす場合に限り表2のカテゴリーに分類されている。
4. EC閣僚理事会指令ではbar，barnおよび「血圧の単位」mmHgを表2のカテゴリーに入れている。

換算表

力	N(=10^5 dyn)	kgf	lbf
	1	0.101972	0.224809
	9.80665	1	2.20462
	4.44822	0.453592	1

粘度　1 Pa·s(N·s/m^2) = 10 P(ポアズ)(g/(cm·s))

動粘度　1 m^2/s = 10^4 St(ストークス)(cm^2/s)

圧力	MPa(=10 bar)	kgf/cm^2	atm	mmHg(Torr)	lbf/in^2(psi)
	1	10.1972	9.86923	7.50062 × 10^3	145.038
	0.0980665	1	0.967841	735.559	14.2233
	0.101325	1.03323	1	760	14.6959
	1.33322 × 10^{-4}	1.35951 × 10^{-3}	1.31579 × 10^{-3}	1	1.93368 × 10^{-2}
	6.89476 × 10^{-3}	7.03070 × 10^{-2}	6.80460 × 10^{-2}	51.7149	1

エネルギー・仕事・熱量	J(=10^7 erg)	kgf·m	kW·h	cal(計量法)	Btu	ft·lbf	eV
	1	0.101972	2.77778 × 10^{-7}	0.238889	9.47813 × 10^{-4}	0.737562	6.24150 × 10^{18}
	9.80665	1	2.72407 × 10^{-6}	2.34270	9.29487 × 10^{-3}	7.23301	6.12082 × 10^{19}
	3.6 × 10^6	3.67098 × 10^5	1	8.59999 × 10^5	3412.13	2.65522 × 10^6	2.24694 × 10^{25}
	4.18605	0.426858	1.16279 × 10^{-6}	1	3.96759 × 10^{-3}	3.08747	2.61272 × 10^{19}
	1055.06	107.586	2.93072 × 10^{-4}	252.042	1	778.172	6.58515 × 10^{21}
	1.35582	0.138255	3.76616 × 10^{-7}	0.323890	1.28506 × 10^{-3}	1	8.46233 × 10^{18}
	1.60218 × 10^{-19}	1.63377 × 10^{-20}	4.45050 × 10^{-26}	3.82743 × 10^{-20}	1.51857 × 10^{-22}	1.18171 × 10^{-19}	1

1 cal = 4.18605 J（計量法）

= 4.184 J （熱化学）

= 4.1855 J （15 °C）

= 4.1868 J（国際蒸気表）

仕事率　1 PS（仏馬力）

= 75 kgf·m/s

= 735.499 W

放射能	Bq	Ci
	1	2.70270 × 10^{-11}
	3.7 × 10^{10}	1

吸収線量	Gy	rad
	1	100
	0.01	1

照射線量	C/kg	R
	1	3876
	2.58 × 10^{-4}	1

線量当量	Sv	rem
	1	100
	0.01	1

（86年12月26日現在）

A STUDY ON DENSITY, MELTING POINT, THERMAL EXPANSION, CREEP, THERMAL DIFFUSIVITY AND THERMAL CONDUCTIVITY OF THE SIMULATED ROCK-LIKE OXIDE (ROX) FUELS